Systems/Circuits

Discharge and Role of GABA Pontomesencephalic Neurons in Cortical Activity and Sleep-Wake States Examined by Optogenetics and Juxtacellular Recordings in Mice

Youssouf Cissé,[1] Masaru Ishibashi,[2] Josefa Jost,[1] Hanieh Toossi,[1] Lynda Mainville,[1] Antoine Adamantidis,[3] Christopher S. Leonard,[2] and Barbara E. Jones[1]

[1]Department of Neurology and Neurosurgery, Montreal Neurological Institute, McGill University, Montreal, Quebec H3A 2B4, Canada, [2]Department of Physiology, New York Medical College, Valhalla, New York 10595, and [3]Department of Biomedical Research and Department of Neurology, Zentrum Für Experimentelle Neurologie, Inselspital University Hospital Bern, University of Bern, Bern 3010, Switzerland

The cholinergic neurons in the pontomesencephalic tegmentum have been shown to discharge in association with and promote cortical activation during active or attentive waking and paradoxical or rapid eye movement sleep. However, GABA neurons lie intermingled with the cholinergic neurons and may contribute to or oppose this activity and role. Here we investigated *in vitro* and *in vivo* the properties, activities, and role of GABA neurons within the laterodorsal tegmental and sublaterodorsal tegmental nuclei (LDT/SubLDT) using male and female transgenic mice expressing channelrhodopsin-(*ChR2*)-*EYFP* in vesicular GABA transporter (*VGAT*)-expressing neurons. Presumed GABA (pGABA) neurons were identified by response to photostimulation and verified by immunohistochemical staining following juxtacellular labeling *in vivo*. pGABA neurons were found to be fast-firing neurons with the capacity to burst when depolarized from a hyperpolarized membrane potential. When stimulated *in vivo* in urethane-anesthetized or unanesthetized mice, the pGABA neurons fired repetitively at relatively fast rates (~40 Hz) during a continuous light pulse or phasically in bursts (>100 Hz) when driven by rhythmic light pulses at theta (4 or 8 Hz) frequencies. pNon-GABA, which likely included cholinergic, neurons were inhibited during each light pulse to discharge rhythmically in antiphase to the pGABA neurons. The reciprocal rhythmic bursting by the pGABA and pNon-GABA neurons drove rhythmic theta activity in the EEG. Such phasic bursting by GABA neurons also occurred in WT mice in association with theta activity during attentive waking and paradoxical sleep.

Key words: **EEG; paradoxical sleep; REM sleep; slow wave sleep; theta; waking**

Significance Statement

Neurons in the pontomesencephalic tegmentum, particularly cholinergic neurons, play an important role in cortical activation, which occurs during active or attentive waking and paradoxical or rapid eye movement sleep. Yet the cholinergic neurons lie intermingled with GABA neurons, which could play a similar or opposing role. Optogenetic stimulation and recording of these GABA neurons in mice revealed that they can discharge in rhythmic bursts at theta frequencies and drive theta activity in limbic cortex. Such phasic burst firing also occurs during natural attentive waking and paradoxical sleep in association with theta activity and could serve to enhance sensory-motor processing and memory consolidation during these states.

Received Dec. 3, 2019; revised May 5, 2020; accepted June 16, 2020.

Author contributions: Y.C., A.A., C.S.L., and B.E.J. designed research; Y.C., M.I., and L.M. performed research; Y.C., M.I., J.J., H.T., C.S.L., and B.E.J. analyzed data; Y.C., M.I., L.M., A.A., and C.S.L. edited the paper; A.A. contributed unpublished reagents/analytic tools; C.S.L. and B.E.J. wrote the paper.

This work was supported by Canadian Institutes of Health Research Grant CIHR MOP130502 to B.E.J. and Grant CIHR MOP246264 to A.A., and National Institutes of Health Grant NIH NS27881 to C.S.L. We thank Sonia Jego and Stephen Glasgow for contributions to the early stages of this research at the Douglas Hospital Research Institute of McGill University.

Y. Cissé's present address: Laboratory of Molecular Life Science, Institute of Biomedical Research and Innovation, Kobe Hybrid Business Center #201, 6-7-6, Minatojima-Minamimachi Chuo-ku, Kobe, 650-0047 Japan.

M. Ishibashi's present address: Department of Neurophysiology, Hamamatsu University School of Medicine, 20-1 Handayama 1-chome, Higashi-ku, Hamamatsu, Shizuoka 431-3192, Japan.

The authors declare no competing financial interests.

Correspondence should be addressed to Barbara E. Jones at barbara.jones@mcgill.ca.

https://doi.org/10.1523/JNEUROSCI.2875-19.2020

Introduction

Neurons in the pontomesencephalic tegmentum (PMT) have long been known to play a critical role in stimulating cortical activation during waking and paradoxical sleep (PS) or rapid eye movement sleep, particularly the cholinergic neurons (El Mansari et al., 1989; Steriade et al., 1990, 1991; Jones, 1991, 1993; Brown et al., 2012). Yet the ACh neurons are intermingled with other GABA and glutamate neurons in the laterodorsal tegmental, sublaterodorsal (LDT/SubLDT) and pedunculopontine tegmental nuclei (PPT) (Ford et al., 1995; Wang and Morales, 2009), which may contribute to this role. It has thus been important to record from immunohistochemically identified neurons in this region, which has been possible, though exceedingly difficult, to do using juxtacellular recording and postmortem identification of singly labeled neurons (Boucetta et al., 2014). To facilitate and extend these studies, we sought to use cell type-specific optogenetic mice (Zhao et al., 2011), which through expression of channelrhodopsin-2 (ChR2), would allow *in vitro* and *in vivo* photostimulation and identification first of ACh neurons, as previously published (Cisse et al., 2018) and here in the present study, of GABA neurons in the LDT/SubLDT.

Cortical activation is characterized by fast activity on the EEG, particularly in the γ band (30-60 Hz and above), during active or attentive waking (aW) and PS (Maloney et al., 1997). It is also characterized by rhythmic theta activity (6-10 Hz) in the hippocampus and limbic cortex, including the retrosplenial cortex (Maloney et al., 1997; Koike et al., 2017). Both γ and theta activity in the cortex is modulated by input from cholinergic and noncholinergic, including GABA, neurons in the basal forebrain (Cape and Jones, 2000; Cape et al., 2000; Lee et al., 2005; Hassani et al., 2009; Brown et al., 2012; Kim et al., 2015). It has also been known that forebrain theta along with γ can be modulated by brainstem circuits, first thought to be only by tonic and not phasic rhythmic input from the pontomesencephalic reticular formation and/or cholinergic neurons (Vertes and Kocsis, 1997). Using *ChAT-ChR2-EYFP* transgenic (TG) mice, we recently established by applying optogenetic stimulation together with juxtacellular recording that ACh neurons in the LDT/SubLDT and PPT can promote both γ and theta activity in association with aW and PS by tonic and/or phasic discharge (Cisse et al., 2018). Here, we explored further whether GABA neurons in the LDT/SubLDT might also be able to drive theta and discharge in association with theta to promote γ and theta activity in the cortex. We thus used vesicular GABA transporter *(VGAT)-ChR2-EYFP TG* mice for optogenetic stimulation, recording, and identification of the GABA neurons, while also using juxtacellular labeling for immunohistochemical verification of the GABA cell type in the LDT/SubLDT, to study the relationship of the GABA cell discharge to EEG activity across sleep-wake states.

Materials and Methods

Animals. Recording experiments were performed *in vitro* and *in vivo* using male and female TG mice, which were bred to express ChR2 fused to EYFP in GABA, VGAT-expressing neurons (abbreviated as *VGAT-ChR2-EYFP* mice), along with *WT C57BL/6* mice of both sexes. The parental strains of the TG mice were obtained from The Jackson Laboratory for Cre-inducible ChR2-EYFP (http://jax.org/strain/012569 or https://www.jax.org/strain/024109) and for *VGAT-IRES-Cre* mice (https://www.jax.org/strain/028862). The WT mice came from Charles River (http://criver.com/products-services/basic-research/find-a-model/c57bl-6n-mouse). The original development and experimental use of cell type-specific optogenetic TG mice demonstrated how they could be effectively used for the electrophysiological and behavioral study of central ACh and GABA neurons (Zhao et al., 2011). For the *in vitro* studies, all procedures complied with National Institutes of Health guidelines and were approved by New York Medical College Institutional Animal Care and Use Committee. For the *in vivo* studies, all procedures complied with Canadian Institutes of Health Research guidelines and were approved by the McGill University Animal Care Committee and the Canadian Council on Animal Care.

In vitro recording in brain slices. Brain slices (250 μm) were prepared from *VGAT-ChR2-EYFP* (P15-P16) mice according to previously published methods (Ishibashi et al., 2015). Briefly, slices were cut with a vibratome (VT1000s, Leica Microsystems) using ice-cold, oxygenated ACSF containing the following (in mM): 124 NaCl, 3 KCl, 1.2 NaH_2PO_4, 2 $CaCl_2$, 2 $MgSO_4$, 26 $NaHCO_3$, and 10 dextrose (295-305 mOsm). Slices were then incubated for 10 min in an N-methyl-D-glucamine recovery solution (Ting et al., 2014) at room temperature containing the following (in mM): 115 N-methyl-D-glucamine-Cl, 2.5 KCl, 1.2 $NaHPO_4$, 0.5 $CaCl_2$, 10 $MgSO_4$, 25 $NaHCO_3$, and 25 dextrose (295-305 mOsm) before being rinsed (5×) and then stored in continuously oxygenated room temperature ACSF in the dark. Whole-cell recordings were obtained using an Axopatch 200B amplifier and borosilicate micropipettes (2-4 MΩ) in a submersion chamber holding a slice that was superfused at 1-2 ml/min with oxygenated room temperature ACSF. EYFP fluorescence was found to be inadequate to clearly visualize and select ChR2-EYFP-labeled cells. The neurons were thus visualized for patching using near-infrared DIC optics on a fixed-stage microscope (Olympus BX50WI) with a 40× (NA 0.8) objective and selected according to their relatively small size (long axis < 20 μm) compared with cholinergic neurons (Ford et al., 1995; Brown et al., 2008). The pipette solution contained the following (in mM): 144 K-gluconate, 3 $MgCl_2$, 10 HEPES, 0.3 NaGTP, 4 Na_2ATP (310 mOsm) and bis-fura 2 (50 μM; Invitrogen) for calcium chelation. Biotinylated Alexa-594 (15 μM; Invitrogen) was also included in the pipettes in all experiments for structural labeling of recorded cells. A sample of these cells was used to measure soma size from fluorescent images of the Alexa-594-filled cells in the slices. All recorded cells were located in the LDT as determined from a low-power (4× objective) observation of the slice. All cells that responded with photocurrents were considered to be presumptive GABA (pGABA) neurons. For photostimulation, a transistor-transistor logic (TTL)-gated, 473 nm laser (100 mW; SLOC) was coupled to an optic fiber (200-μm-diameter core, 0.22 NA) that was positioned 1.0–1.5 mm above the LDT region of the slice. Imaging, laser-gating, control of the Axopatch 200B and acquisition of current and voltage signals were accomplished using custom software (TIWB) (Inoue, 2018) running on a MacOS computer via an ITC-18 interface board (HEKA). Whole-cell data were analyzed using Igor Pro 8 (Wavemetrics). Spike shape and repetitive firing were analyzed using custom Igor routines previously described (Erisir et al., 1999). Briefly, spike width was taken as the duration at half the amplitude between spike threshold and spike peak. Spike time for computing instantaneous firing frequency (IFF) was taken as the time the spike crossed 0 mV. Spike latencies were measured from the onset of the laser-gating TTL pulse to the foot of the action potential. All reported values of V_m were corrected by −15 mV to compensate for the measured liquid junction potentials and average values are reported as mean ± SEM.

In vivo recording in mice. Mice were housed under a 12:12 h light-dark schedule with lights on from 7:00 A.M. to 7:00 P.M. and had free access to food and water. Adult TG and WT mice (25–30 g) were used for acute recording studies with anesthesia or for chronic recording studies without anesthesia using head fixation following surgical implantation of a head fixation post.

For recordings in TG and WT anesthetized (A) mice, anesthesia was induced with isoflurane administered within a Plexiglas box (~5%) and then maintained through a mask (~2.5%) during surgery. Body temperature was maintained at 36°C–37°C by a thermostatically controlled heating pad through a rectal thermal probe. The mice were positioned in a stereotaxic frame (David Kopf Instruments) for both surgery and subsequent recording. To record activity of the EEG, stainless-steel screws were placed bilaterally over the retrosplenial cortex 1.0 mm posterior

and 0.5–0.65 mm lateral to bregma and unilaterally in the frontal bone as a reference. Two holes were opened in the skull over the region of the lambdoid suture: one for the optic fiber and one for the recording micropipette. Following resection of the dura mater in each hole, the isoflurane was diminished and replaced by urethane (ethyl carbamate, Sigma Millipore) using an initial large dose (1 g/kg, i.p.) followed by supplementary small doses (0.1–0.15 g/kg), if necessary during the recording, as indicated by the presence of a withdrawal response of the limb to pinch. The animal was transferred in the stereotaxic apparatus to the recording chamber where the optic fiber (200 µm, 0.22 NA, Thorlabs) was inserted at ~1 mm posterior and ~3 mm lateral to λ and descended at a 40° angle from vertical in the coronal plane ~2.0-2.5 mm from the brain surface through the inferior colliculus to stop at a position dorsal and lateral to the LDT/SubLDT (Fig. 1). EEG and unit recording then proceeded as in the chronic studies (below).

For recordings in the TG and WT unanesthetized (UA) mice, the animals were first operated for implantation of electrodes and a head fixation post. For this surgery, anesthesia was induced (5%) and maintained with isoflurane (~2.5%, as above). As for the TG-A mice, screws were implanted over the retrosplenial cortex (above) and frontal bone for EEG and embedded in acrylic cement into which the metal head fixation post was also fixed. The EEG wires were sent to a connector fixed to the left side of the head. As for the TG-A mice, the skull was cleaned in the region around the lambdoid suture. A hole was drilled for the placement of an indwelling fiber optic cannula (200 µm core, 0.22 NA, Thorlabs) according to the coordinates of the optic fiber (above). Acrylic cement was applied to surround the cannula while leaving a small area of the skull around the lambdoid suture clean but covered for subsequent opening to insert the micropipette at the time of recording. Following recovery from the surgery (~3–5 d), the mice were introduced to the head fixation apparatus in which their headpost was inserted into a receptacle while their body was comfortably contained within a tube lined with foam rubber. The time of habituation to the head fixation was gradually increased from ~30 min up to ~5 h over a period of 10–15 d until the mice would be quietly awake or asleep during the afternoon period of recording, which is their normal maximal sleeping period. Following complete habituation, the mice were anesthetized again with isoflurane (above) to drill the hole in the region of the lambdoid suture for insertion of the micropipette (above). The mouse was returned to its home cage until the next day.

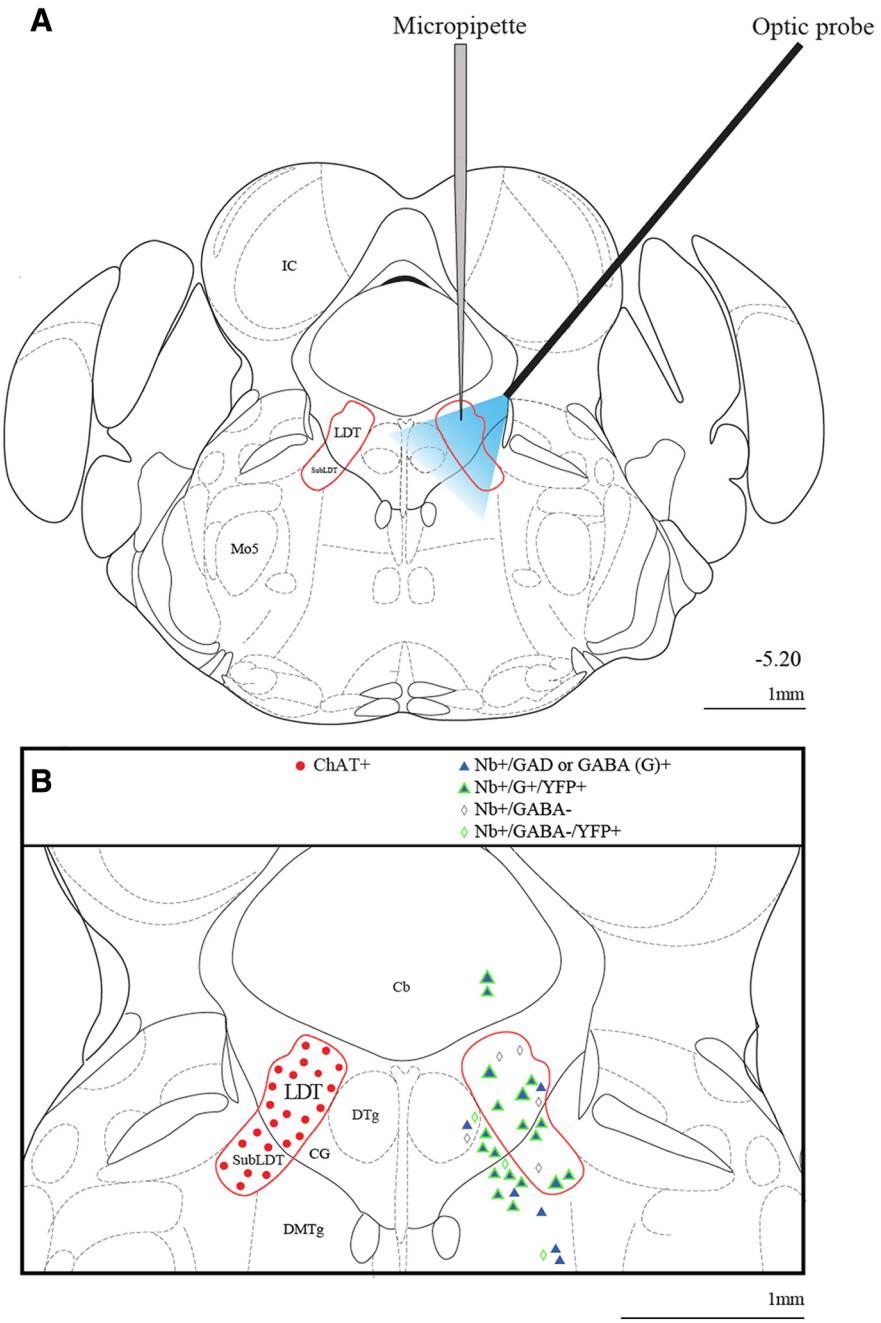

Figure 1. Photostimulation with juxtacellular recording and labeling of pGABA neurons in *VGAT-ChR2-EYFP TG* mice. GABA neurons were targeted for recording and photostimulation *in vitro* in LDT and *in vivo* in LDT/SubLDT. ***A***, Approximate position of the optic fiber and the estimated distribution of blue light *in vivo* are shown reaching the LDT/SubLDT at a 40° angle and the Nb-filled micropipette at 90°. ***B***, Left, Distribution of ChAT-immunopositive, ACh neurons was restricted to the LDT and SubLDT nuclei. Right, Nb-labeled neurons are plotted, which were retrieved from juxta-submitted, responding or pGABA units within the LDT/SubLDT or adjacent areas of TG-A ($n = 34$) and TG-UA ($n = 12$) mice. Shown with different symbols are the Nb-labeled neurons (Nb^+), which were G-positive (filled blue triangles represent GAD- or GABA-immunopositive) or $GABA^-$ (black open diamonds represent GABA-immunonegative) and which were ChR2-$EYFP^+$ (green outline represents YFP^+) or ChR2- $EYFP^-$. Large symbols represent the Nb-labeled/G^+/ChR2-$EYFP^+$ cells shown in Figure 2*A–D*. Neurons were plotted onto one atlas level representing the central level for the LDT/SubLDT (~−5.20 from bregma). Cb, cerebellum; CG, central gray; DMTg, dorsomedial tegmental area; DTg, dorsal tegmental nucleus; IC, inferior colliculus; LDT, lateral dorsal tegmental nucleus; Mo5, motor trigeminal nucleus; SubLDT, sublaterodorsal tegmental nucleus. Plates adapted from Paxinos and Franklin (2001). Scale bars, 1 mm.

In vivo unit recording and labeling. On the day of recording, the TG-UA and WT-UA mice were placed in the head fixation apparatus. The dura mater inside the hole was superfused with lidocaine and incised to allow descent of the micropipette to the LDT/SubLDT. The TG-A, TG-UA, and WT-UA mice were subsequently transferred within the stereotaxic apparatus to the recording chamber. The optic fiber was lowered at a 40° angle through brain tissue in the TG-A mice, as above, and the optic fiber patch cable was attached to the indwelling fiber optic cannula in the TG-UA and WT-UA mice. For recording, a glass micropipette (~1 µm tip, ~40 MΩ) filled with ~5%

Neurobiotin (Nb; Vector Laboratories) in 0.5 M NaCl solution was lowered vertically at ~1 mm posterior and 0.5–1.3 mm lateral to λ using a Kopf micropositioner (model 660, David Kopf Instruments) to target the LDT/SubLDT (Fig. 1). Single units were recorded and labeled using an intracellular amplifier (Neurodata IR-283A, Cygnus Technology). The unit signal was amplified (2000×), digitized at a sampling rate of 8 kHz, and filtered (bandpass filter: 0.3–3 kHz) using a CyberAmp 380 (Molecular Devices) and acquired for online viewing with the Axoscope software (version 10.1, Molecular Devices). The unit was simultaneously recorded with EEG (sampled at 250 Hz and filtered between 0.5–100 Hz) in TG-UA and WT-UA mice and together with video of the animal's head in TG-UA mice, using Harmonie software (version 5.2, Stellate).

Photostimulation with blue light (473 nm) was applied through the optic fiber (~200 μm core diameter, 0.22 NA, Thorlabs) using a laser (Laserglow Technologies, LRS-0473-PFM-00-100-05, >100 mW) connected to a TTL-gated power supply (R471005FX), which was in turn connected to a pulse signal generator (Master 8, AMPI). The laser power for stimulation was set in the TG-A mice to ~40 mW, which would correspond to ~14 mW mm^{-2} at 1 mm from the tip (https://web.stanford.edu/group/dlab/cgi-bin/graph/chart.php) aimed at the dorsolateral border of the central gray adjacent to the LDT/SubLDT cholinergic and intermingled GABA cells (Fig. 1). In the TG-UA mice, the laser power had to be considerably reduced, since even short pulses at ~40 mW elicited movements with arousal. In searching for responding units in these mice, short pulses with a power of ~10 mW were used and then reduced to levels that continued to elicit a spike but without the movement or ostensible behavioral arousal of the mouse. In this process, the light pulse generally had to be reduced to levels between 5.0 and 0.5 mW. With this predetermined setting for each mouse, short light pulses (SLPs) of 2-15 ms were delivered to test systematically whether the unit emitted a spike within 15 ms over several trials. Units were subsequently examined in association with EEG activity to a long (~1-5 s) continuous light pulse (CLP) and/or to rhythmic light pulses (RLPs) at low theta frequency in TG-A mice (100 ms pulse at 4 Hz for ~5 s) and at high theta frequency in TG-UA mice (50 ms at 8 Hz for ~5 s). The response to photostimulation was also tested in WT-UA mice serving as controls. In a number of WT-UA animals, units together with EEG were recorded during undisturbed natural sleeping-waking.

Following characterization, units were submitted to juxtacellular labeling using positive current pulses (1-10 nA, 200 ms) delivered for a period of ~2 min (Pinault, 1996). In any 1 mouse, multiple units were selected for submission to juxtacellular labeling. In the initial experiments in TG-A mice, several (3-12) units were selected during the recording by whether they appeared or not to emit a spike during the SLP of ≤ 15 ms over several trials; however, on offline analysis, some units proved to have not responded consistently, thus resulting in juxtacellular submission of both responding and nonresponding units in some mice. In the subsequent studies in the TG-UA mice, units were more precisely selected for labeling such that only a few (1-3) units that were clearly either responding or nonresponding in any 1 mouse were submitted to juxtacellular labeling. Following offline analysis, each unit was confirmed as responding or not responding to the SLP and thus classified as pGABA or pNon-GABA (below). For quantitative analysis of juxtacellular labeling, Nb-labeled neurons were only tabulated from mice in which only pGABA or only pNon-GABA neurons were juxta-submitted.

At the end of the recording session (~5 h), the TG or WT A mice were administered an overdose of urethane (3 g/kg, i.p.) and the UA mice of sodium pentobarbital (Euthanyl, 100 mg/kg, i.p., Bimeda-MTC Pharmaceuticals) and perfused transcardially with 100 ml of cold saline, followed by 200 ml of cold 3% PFA solution for fixation of the brain with death. The brains were removed, postfixed overnight in the fixative solution, and immersed for 2-3 d in 30% sucrose in PB for cryoprotection. They were frozen at −50°C and stored at −80°C.

In vivo electrophysiological signal analysis. Simultaneously recorded unit and EEG signals from TG and WT mice were processed using MATLAB (R2011b, The MathWorks) with programs previously developed and described for unit recording in urethane-anesthetized rats (Manns et al., 2000; Boucetta and Jones, 2009) and unanesthetized head-fixed rats (Lee et al., 2005; Boucetta et al., 2014). The mean latency to spike during the SLP was calculated across 3 SLPs for each unit. Spike width or duration was determined from the average of all spikes and was measured from the initial positive deflection to the return to baseline following the secondary negative deflection or "second zero crossing" (where the crossing was measured at 10% of the peak amplitude of the wave above and below the initial baseline or "zero" to avoid slight variations in "zero" on return to baseline). Accordingly, unit average discharge rate (ADR), IFF (the reciprocal of the modal interspike interval [ISI]), and autocorrelation function were calculated together with the EEG power spectrum and unit-to-EEG cross-correlated activity from spike-triggered averages (STAs). These measures were computed for the ~5 s periods before and during the CLP and RLP stimulations. In addition, integrated average amplitude of EEG frequency band activity was computed for δ (0.5–3.5 Hz in TG-A mice and 0.5–4.0 Hz in TG- and WT-UA mice) and γ (30-58 Hz). In UA mice, low (4.0–6.0) and high (6.0–10 Hz) theta frequency band activities were also computed. These measures were collected for the experiments involving photostimulation in TG-A and TG-UA mice and in WT-UA mice as controls as well as for periods of natural sleep-wake states.

Histochemistry. Brains from the *in vivo* studies were cut in serial sections at 25 μm thickness on a freezing microtome. Sections were collected through the PMT for staining of Nb. They were incubated for 2.5 h in Cy3-conjugated streptavidin (SA-Cy3, 1:1000, catalog # 016-160-084, RRID:AB_2337244, Jackson ImmunoResearch Laboratories), mounted, and coverslipped with glycerol for examination under the fluorescence microscope. Sections containing Nb-labeled cells along with other sections through the region of the LDT/SubLDT were then removed from the slides and processed for immunofluorescent staining. The presence of ChR2-EYFP in neurons was assessed by the native fluorescence of the YFP.

For identifying GABA neurons, an antibody for glutamic acid decarboxylase (GAD, mouse anti-GAD67, 1:250, Millipore, catalog #MAB5406, RRID:AB_2278725) was used in many of the TG-A mice or for GABA (rabbit anti-GABA, 1:2000, Sigma Millipore, catalog #A2052, RRID:AB_477652) in the remainder TG-A and in all TG-UA and WT-UA mice. Following incubation with the primary antibodies overnight, the sections were rinsed and incubated for 2 h in appropriate combinations of cyanine-conjugated (Cy5) secondary antibodies from donkey (Jackson ImmunoResearch Laboratories): Cy5-conjugated anti-mouse (1:800, catalog #715-175-150, RRID:AB_2340819) or Cy5-conjugated anti-rabbit (1:800, catalog #711-175-152, RRID:AB_2340607). Finally, sections were rinsed, mounted, and coverslipped with glycerol.

Fluorescent image analysis. Processed sections were viewed using a DMLB microscope (Carl Zeiss) equipped with fluorescence filters for excitation and emission of Cy2, Cy3, and Cy5 dyes, a digital camera (Orca-R^2, C10600-10B, Hamamatsu photonics KK) and an *x*/*y*/*z* motorized stage. The serial sections were first stained for Nb using Cy3 as chromogen. Then following examination, those in which Nb-labeled cells were found were immunostained for GAD or GABA using Cy5. Low (5×) and high (40×) magnification images were acquired through the regions of the Nb-labeled cells using StereoInvestigator software (MicroBrightField, MBF) to allow subsequent mapping and assessment of each Nb-labeled cell as being positive or negative for EYFP (as native YFP fluorescence) and for GABA (as GAD or GABA immunofluorescence). Positive staining was evaluated from YFP staining over the plasma membrane of the cell for EYFP, and from Cy5 staining in the cytoplasm of the cell for GAD or GABA. Evaluation of Nb, EYFP, and GABA staining was judged by three observers. In addition, images from 1 to 3 sections through the LDT/SubLDT from each brain were acquired for immunostaining to estimate the percentage of GABA neurons, which were positive for EYFP, and that of $EYFP^+$ neurons, which were positive or negative for GABA in the brains of the TG mice.

Statistical analysis and representation of data. From the *in vivo* studies, electrophysiological and histochemical data were prepared and analyzed using MATLAB (R2011b, The MathWorks) and SYSTAT (SYSTAT Software, version 13). The proportion of units that were submitted to the juxtacellular labeling protocol (juxta-submitted), which were labeled for Nb along with the proportion of these which were $GABA^+$ or $GABA^-$ and $EYFP^+$ or $EYFP^-$ were computed per mouse.

For the analysis of the recorded units, the electrophysiological data for all recorded and juxta-submitted units was computed. In offline analysis, units were classified as having responded or not responded by emitting a spike during the 15 ms SLPs and accordingly considered as pGABA or pNon-GABA neurons. The average latency to spike was computed during three SLPs for each pGABA neuron. For assessment of whether these units corresponded to immunohistochemically identified Nb-labeled GABA or Non-GABA neurons, it was necessary to consider them as a group per mouse, since not all juxta-submitted units were Nb-labeled and not all Nb-labeled cells were $GABA^+$ or $GABA^-$ in each brain. Accordingly, if on offline analysis, all juxta-submitted units in a brain were classified as pGABA or pNon-GABA, they were considered as a group.

Measurements were compared statistically using Student's *t* tests or in some cases one-way ANOVA repeated-measures along with multiple paired *t* tests with Bonferroni corrections (SYSTAT 13). Figures were prepared using MATLAB and Adobe Illustrator and Photoshop (Adobe Creative Suite, CS4).

Results

Photostimulation and identification of GABA neurons in *VGAT-ChR2-EYFP TG* mice

Neurons were recorded and photostimulated in *VGAT-ChR2-EYFP* TG mice in the region of the LDT/SubLDT nuclei where ACh neurons are clustered in the PMT (Fig. 1). In these nuclei, cells that were GAD- or GABA-immunoreactive (G-positive) could be seen to manifest intrinsic YFP in the brains of *VGAT-ChR2-EYFP* mice. Nonetheless, the proportion of G^+ cells that manifested YFP could not be estimated, since the YFP was only visible in the cell plasma membrane, where the ChR is inserted and functions as a light-sensitive cation channel (Nagel et al., 2003). The YFP was thus difficult to resolve in the small GABA neurons within the LDT/SubLDT region. Such assessment was thus only undertaken in the Nb-labeled cells (below).

Putative GABA neurons were studied electrophysiologically in *VGAT-ChR2-EYFP TG* mice *in vitro* within the LDT in brain slices and *in vivo* within the LDT/SubLDT in both anesthetized mice (TG-A, $n = 6$) and unanesthetized, head-fixed, naturally sleeping-waking mice (TG-UA, $n = 9$) (Fig. 1). Based on previous studies (Cisse et al., 2018) and the current *in vitro* findings (below), units that emitted a spike during light pulses of $\leq$15 ms were identified *in vivo* as pGABA units. Of the units sampled and selected for recording *in vivo* in the LDT/SubLDT region ($n = 144$ in 15 mice), 63% were considered to be pGABA units ($n = 91$) and the remainder, which did not respond, pNon-GABA units ($n = 53$). A number of the responding units ($n = 68$ or ~87% of the total) and nonresponding units ($n = 10$ or ~13% of the total) were selected for being submitted to juxtacellular labeling (juxta-submitted). Of the juxta-submitted units, ~70% were successfully labeled with Nb (Nb-labeled, $n = 57$); and of the Nb-labeled cells, only a slight majority was GAD- or GABA-immunopositive ($n = 28$ or ~52%) and the rest GAD- or GABA-immunonegative negative ($n = 26$ or ~48%). Of the responding neurons from mice in which only responding units were juxta-submitted, 20 or 59% of the Nb-labeled cells ($n = 37$) were identified as GAD- or GABA-immunopositive (G^+; Fig. 1*B*). Given, however, that the assessment of G positivity can be problematic, particularly with GAD immunostaining and thus yield false-negative assessments, we reconsidered $GABA^+$ estimates to only include those cells immunostained for GABA (Table 1). In these cases of responding units, 13 or 68% of the Nb-labeled cells ($n = 19$) were GABA-immunopositive. Of the nonresponding units from mice in which only nonresponding units were juxta-submitted, 1 or 20% of the Nb-labeled cells ($n = 5$) were $GABA^+$.

Table 1. Number and percent of responding, pGABA, and nonresponding, pNon-GABA, units, which were Nb-labeled, GABA-immunoreactive, and/or $EYFP^+$[a]

Units	Nb^+ cells	$GABA^+/Nb^+$	$EYFP^+/Nb^+GABA^+$	$GABA^+/Nb^+EYFP^+$
Responding[b] pGABA	19	68%	69%	90%
Nonresponding[c] pNon-GABA	5	20%	0%	0%

[a]Number of Nb^+ cells that were recorded in 9 mice in which only responding or nonresponding units were submitted to juxtacellular labeling and were, respectively, considered to be pGABA or pNon-GABA units. Only Nb-labeled cells that were immunostained for GABA are included.
[b]Responding neurons emitted a spike during $\leq$15 ms light pulses.
[c]Nonresponding neurons did not emit a spike within 15 ms light pulses and were in the majority inhibited by light pulses.

We thus concluded that the responding units were comprised in the majority (~70%) by GABA-immunopositive neurons and were thus appropriately considered to be probable or presumed pGABA units, whereas the nonresponding units were comprised in the majority (~80%) by GABA-immunonegative neurons and were thus appropriately considered to be pNon-GABA units.

All Nb-labeled cells were also examined for expression of ChR2-EYFP ($EYFP^+$) by examination of the intrinsic YFP. YFP was clearly visible in the plasma membrane of large GAD^+ cerebellar Purkinje cells, which responded to photostimulation and could be juxtacellularly labeled with Nb (Fig. 2*A*). YFP was much more difficult to discern in the membrane of $GABA^+$, Nb-labeled neurons in the LDT or SubLDT, which were small neurons (Fig. 2*B-D*). Of the responding neurons from mice in which only responding units were juxta-submitted, numerous Nb-labeled neurons immunostained for GAD ($n = 6$) together with those immunostained for GABA ($n = 13$) were identified as Nb-labeled/G^+/$EYFP^+$ neurons (Fig. 1*B*). Among the responding neurons, ~69% of Nb-labeled GABA-immunopositive neurons ($n = 13$) were identified as $EYFP^+$ ($n = 9$; Table 1), whereas ~17% of the Nb-labeled GABA-immunonegative neurons ($n = 6$) were $EYFP^+$ ($n = 1$). Of all the responding Nb-labeled $EYFP^+$ neurons ($n = 10$), 90% were $GABA^+$ ($n = 9$; Table 1). Of the nonresponding units, none of the Nb-labeled $GABA^+$ or $GABA^-$ neurons was identified as $EYFP^+$ (not shown). It was thus confirmed that the majority of the pGABA units were $GABA^+$ and $EYFP^+$, whereas the majority of the pNon-GABA units were $GABA^-$ and $EYFP^-$.

Electrophysiological study of GABA neurons in brain slices of TG mice

Relatively small (long axis < 20 μm) LDT neurons were selected for recording in brain slices from *VGAT-ChR2-EYFP TG* mice (Fig. 3). After forming a tight seal, but before breakthrough, neurons often showed spontaneous action potentials (measured as current transients). In some cells, delivery of 500 ms light pulses (473 nm) elicited reliable repetitive spiking (Fig. 3*A*, left) and brief pulses (2 ms), elicited short latency single or couplets of spikes (Fig. 3*A*, right). Upon breakthrough, it was revealed that these light pulses produced robust depolarizing photocurrents in responsive neurons (Fig. 3*B*, top). When present (21 of 38 neurons), these currents showed a characteristic rapid initial transient (-137 ± 46 pA) that peaked at 11.5 ± 4.8 ms and then relaxed to a steady current (-85 ± 29 pA; $n = 6$). After confirming functional expression of ChR2 in these pGABA neurons, recording was switched to current clamp, under which the photocurrents produced depolarizations (27 ± 4 mV; $n = 6$) that were large enough to evoke repetitive firing from subthreshold

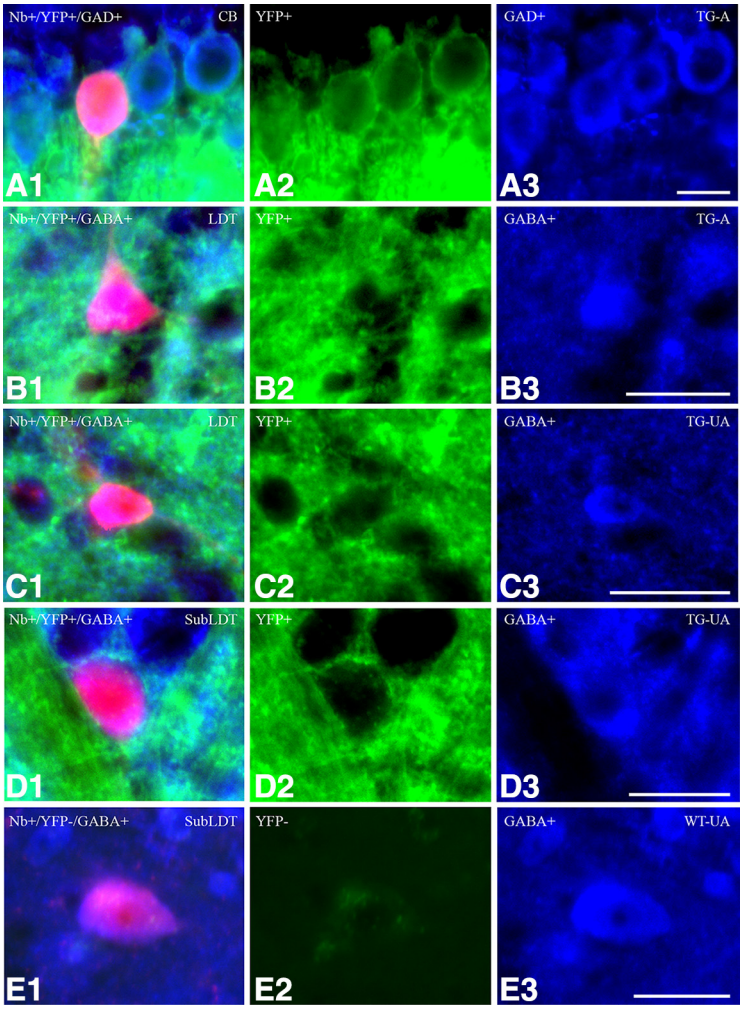

Figure 2. Fluorescent images of recorded and Nb-labeled GABA neurons. Neurons that were recorded and labeled with Nb (red) were identified as GABA neurons by immunofluorescent staining for GAD or GABA (blue). ***A***, Large Purkinje cell, which was recorded and juxta-labeled with Nb in a TG-A mouse (Mouse VGAT77) in which all juxta-submitted units responded to a SLP and were thus considered pGABA units. The Nb^+ neuron along with adjacent Purkinje cells were immunopositive for GAD and manifested clear YFP fluorescence in the plasma membrane reflecting ChR2-EYFP expression. ***B***, Small recorded and Nb-labeled neuron in the LDT of a TG-A mouse (Mouse VGAT81) in which all juxta-submitted units were pGABA. The Nb^+ neuron was GABA-immunopositive and appeared to show some YFP fluorescence over the plasma membrane. ***C***, Small recorded and Nb-labeled neuron in the LDT of a TG-UA mouse (Mouse CVGAT9) in which all juxta-submitted units were pGABA. The Nb^+ neuron was $GABA^+$ and appeared to show YFP fluorescence over the plasma membrane. ***D***, Small recorded, Nb-labeled $GABA^+$ neuron in the SubLDT of a TG-UA mouse (Mouse CVGAT13) in which only pGABA units were juxta-submitted. The $Nb^+/GABA^+$ neuron also manifested YFP fluorescence over the plasma membrane. ***E***, Small recorded, Nb-labeled $GABA^+$ neuron located in the SubLDT of a WT (WT-UA) mouse (Mouse CWT4) in which units that resembled pGABA units and discharged across natural sleep-wake states were juxta-submitted. Scale bars, 20 µm.

membrane potentials (−65.3 ± 1.0 mV; $n = 14$ neurons) (Fig. 3*B*, bottom). With light pulses (2-500 ms), spikes were evoked at a range of latencies (3.3-19.2 ms; $n = 14$ neurons) with a mean of 8.3 ± 1.2 ms (Table 2). At more negative initial membrane potentials, the spike latency became slightly longer, but the number of spikes evoked near pulse onset was greater (Fig. 3*B*, green). With light pulses of 0.5 s applied at a subthreshold membrane potential (V_m −67.7 ± 0.8 mV), the ADR was 18.4 ± 5.9 Hz, and the highest IFF was 57.1 ± 28.8 Hz ($n = 5$; Table 2). With the same pulses applied at lower membrane potentials (initial V_m −83.2 ± 1.6 mV), the ADR was similar (13.3 ± 3.7 Hz), whereas the highest IFF increased significantly to 140.5 ± 40.1 Hz ($n = 5$; $t = 4.11$, df = 4, $p < 0.05$; Table 2), suggesting that subthreshold intrinsic membrane currents augmented the depolarization produced by the photocurrent.

To examine intrinsic firing properties, direct current pulses were delivered from membrane potentials near rest (−65 to −70 mV) for 12 pGABA neurons. In the majority of cells, depolarizing pulses (500 ms) elicited repetitive firing with substantial spike frequency adaptation ($n = 9$ of 12 neurons; Fig. 3*C*) and an initial maximal IFF of 89.9 ± 9.7 spikes/s that slowed to 30.4 ± 4.0 spikes/s during the current pulse (65.0 ± 5.0% adaptation; $n = 9$). The remaining three cells had different firing properties with two firing only transiently at current onset and one firing with an accelerating rate during the current pulse, suggesting a heterogeneity among the pGABA neurons. Responses to hyperpolarizing current pulses confirmed that pGABA neurons typically showed rebound excitation ($n = 10$ of 12; Fig. 3*C*, arrow) that drove spike bursts, which are indicative of a T-type Ca^{2+} current and characteristic of Type I LDT neurons (Leonard and Llinas, 1990; Kamondi et al., 1992). The average maximal IFF during the burst was 110.5 ± 21.7 spikes/s (range: 42-266 spikes/s; $n = 9$), further indicating that at membrane potentials negative to rest, photostimulation of most pGABA neurons could boost firing or drive bursting. Indeed, as the membrane potential was made more negative, brief light pulses (1-2 ms) produced larger and longer depolarizing responses that could produce a spike burst (Fig. 3*D*). pGABA LDT neurons had relatively brief action potentials with a spike width of 0.97 ± 0.05 ms ($n = 16$; Table 2) and an AHP that reached its minimum value shortly after the action potential peak (spike peak to AHP minimum: 3.3 ± 0.3 ms). These features were not different from those measured from other small LDT neurons lacking photocurrents and thus pNon-GABA, whose spike width was 0.92 ± 0.16 ms (Table 2; $n = 5$) and time from spike peak to AHP minimum was 3.46 ± 1.01 ms ($n = 5$; $t = 0.19$, df = 4, $p = 0.86$). In contrast, the spikes of pGABA neurons were significantly more narrow than those of presumed ACh (pACh) LDT neurons, which had a spike width of 1.42 ± 0.06 ms ($n = 13$; $t = 5.9$, df = 27, $p < 0.001$) and a spike peak to AHP minimum of 13.1 ± 1.5 ms ($n = 13$; $t = 7.2$, df = 27, $p < 0.001$) as measured here in the whole-cell slice recordings from *ChAT-ChR2-EYFP* mice previously studied (Cisse et al., 2018). To test firing fidelity in pGABA neurons, we measured spiking in response to trains of 20 light pulses (1-10 ms duration) delivered at different frequencies (1-50 Hz) from subthreshold membrane potentials near −65 mV (Fig. 3*E*). Firing fidelity was high at 1-2 Hz, fell to 60% at 20 Hz and to 40% at 50 Hz (Fig. 3*F*). Being distinct from pACh neurons but not from other small pNon-GABA LDT neurons, the pGABA LDT neurons thus appeared to be relatively fast-firing neurons with brief spikes.

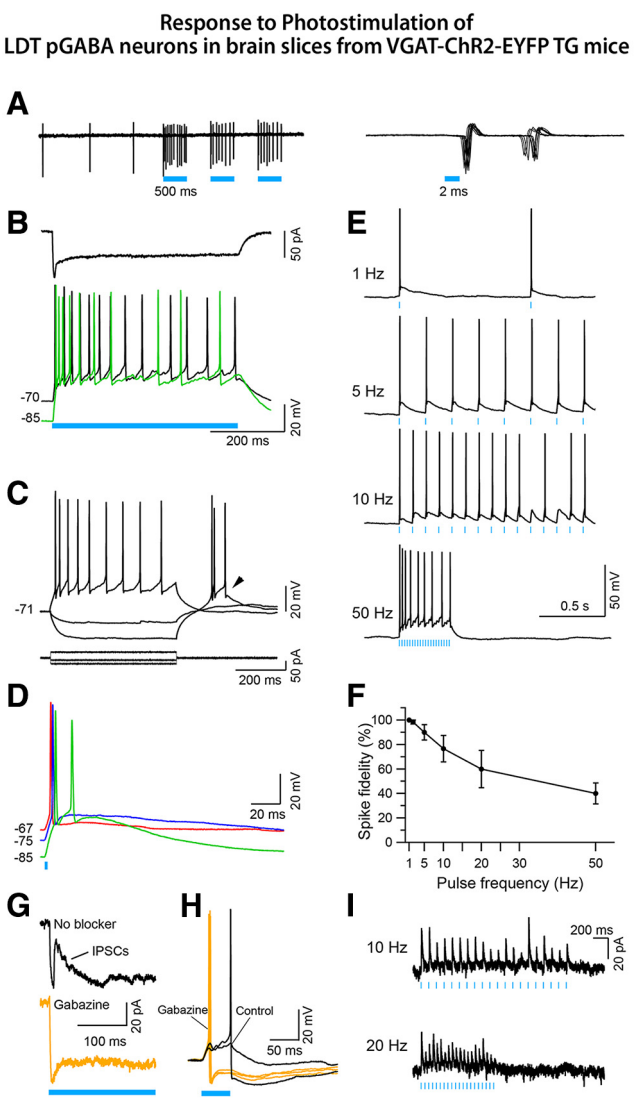

Figure 3. *In vitro* responses of LDT neurons to blue light stimulation in brain slices from *VGAT-ChR2-EYFP TG* mice. ***A***, Tight-seal recording of LDT pGABA neuron. Blue light stimulation (500 ms pulse, blue bars) caused repetitive spiking (left), and brief pulses (2 ms) produced reliable short latency spike couplets (right). ***B***, Top, The characteristic photocurrent measured in voltage-clamp mode (holding potential −65 mV). Bottom, The depolarization and spiking produced by this photocurrent from two subthreshold membrane potentials (black trace, −70 mV; green trace, −85 mV). At −85 mV, the same photocurrent produced higher-frequency firing near the beginning of the pulse. ***C***, Membrane potential responses (top) of the same neuron to injected current pulses (bottom). The intrinsic properties of this pGABA neuron showed rebound low-threshold spiking following the termination of hyperpolarizing current pulses (arrow) typical of T-currents. ***D***, These intrinsic properties shaped responses to brief light pulses (1 ms) by a cell, which fired a single spike from −67 mV (red trace) but fired a couple of spikes from −85 mV (green trace). ***E***, Spiking produced by trains of 20 light pulses (5 ms duration) delivered at 1, 5, 10, and 50 Hz from ~−70 mV for the same cell illustrated in ***B-D***. Blue bars represent the timing and duration of the light pulses. ***F***, Summary of spike fidelity of pGABA LDT neurons versus light pulse frequency (mean ± SEM; $n = 5$). ***G***, In pGABA neurons, IPSCs appeared just after the onset of the inward photocurrent (top, black) and were absent in the presence of gabazine (20 μM; bottom, yellow). ***H***, The presence of photo-evoked IPSCs could delay or block spikes produced by photocurrents (two black traces). Gabazine blocked the IPSCs and shortened the spike latency (three superimposed traces; yellow). ***I***, IPSCs were observed in LDT neurons lacking photocurrents, including putative ACh neurons and reliably followed trains (10 Hz, top; 20 Hz, bottom) of light pulses (10 ms).

In pGABA neurons, photostimulation often produced IPSCs with a latency of 11.7 ± 3.0 ms (range 6.0–34.9 ms; $n = 9$ neurons) that appeared as outward current transients just after the onset of the inward photocurrent (Fig. 3*G*, top, black) and were absent after gabazine application (20 μM; Fig. 3*G*, bottom, yellow). In current-clamp mode, these IPSPs could delay or block spikes produced by the underlying photocurrent (Fig. 3*H*, two black traces). Blocking GABA-A receptors with gabazine (20 μM) shifted these photo-evoked spikes to shorter latencies (Fig. 3*H*, three yellow traces). Laser pulses also produced IPSCs in neurons without photocurrents or pNon-GABA neurons (9 of 12 LDT neurons, including 2 of three cells with long axes > 20 µm; see below) that could reliably follow pulse trains of 10 and 20 Hz (Fig. 3*I*). In contrast to robust photo-evoked IPSCs, there was no evidence of EPSCs that were evoked or modulated by light pulses, although there were clear spontaneous EPSCs in the pNon-GABA neurons.

Table 2. Mean values of spike latency, spike width, unit ADR, and IFF in brain slices or brains of TG, TG-A, TG-UA, or WT-UA (control) mice during current or light pulse stimulation[a]

Group	Units	Latency to spike (ms)	Spike width (ms)	ADR (Hz)	IFF (Hz)
		LP (2-500 ms)[b]	Current pulse[c]	LP (0.5 s)[d]	LP (0.5 s)[d]
TG-Slice	pGABA	8.3 ± 1.2	0.97 ± 0.05	18.4 ± 5.9[e] 13.3 ± 3.7[f]	57.1 ± 28.8[e] 140.5 ± 40.1[f]
		$n = 14$	$n = 16$	$n = 5$	$n = 5$
	pNon-GABA	NA	0.92 ± 0.16	NA	NA
			$n = 5$		
		SLP (≤15 ms)[g]	Spontaneous[h]	CLP (~1-5 s)[i]	CLP (~1-5 s)[i]
TG-A	pGABA	6.01 ± 0.37	1.12 ± 0.03	31.89 ± 3.03	41.86 ± 4.32
		$n = 63$	$n = 59$	$n = 59$	$n = 59$
	pNon-GABA	NA	1.28 ± 0.09	NA	NA
			$n = 23$		
TG-UA	pGABA	5.99 ± 0.67	1.19 ± 0.08	62.52 ± 29.11	116.32 ± 41.74
		$n = 23$	$n = 21$	$n = 8$	$n = 8$
	pNon-GABA	NA	1.42 ± 0.16	NA	NA
			$n = 20$		
WT-UA	pGABA	NA	1.02 ± 0.09	NA	NA
			$n = 11$		

[a]Data are mean ± SEM for number of units indicated.
[b]Light pulses (LP, 2-500 ms) applied in slices from a membrane potential of ~−65 mV for latency to spike.
[c]Spike width measured in slices with current injection.
[d]LPs (0.5 s) applied in slices from different membrane potentials.
[e]from a resting membrane potential of ~−68 mV.
[f]from a hyperpolarized membrane potential of ~−83mV.
[g]SLPs (2-15 ms) applied in mice to examine latency to spike.
[h]Spike width calculated during spontaneous activity in mice.
[i]CLP applied ~5 s in TG-A mice and ~1-5 s in TG-UA mice.

Postrecording measurements from images of cells filled with Alexa-594 within the slice ($n = 26$; not shown) confirmed that neurons with photocurrents were relatively small. Twelve of these filled cells lacked photocurrents, and these included three filled cells with long axes > 20 µm. The somata of the pGABA neurons had estimated long (15.4 ± 0.7 µm) and short (10.5 ± 0.6 µm; $n = 14$) axes that were significantly smaller than those of pACh LDT neurons (long axis 28.1 ± 1.2 µm, $n = 9$; $t = 9.8$, df = 21, $p < 0.001$; short axis 21.3 ± 1.5 µm; $n = 9$; $t = 7.1$, df = 21, $p < 0.001$), as measured here in pACh neurons from *ChAT/ChR2/EYFP* mice previously studied (Cisse et al., 2018).

In conclusion, *in vitro* evidence from *VGAT-ChR2-EYFP TG* mice indicates that, among small LDT neurons, a subset expresses photocurrents and thus ChR2, such as to be considered pGABA neurons. These pGABA LDT neurons manifest the capacity to fire rapidly in a tonic mode but also in high-frequency bursts of spikes. In virtually all such cells, photo-evoked spikes occurred within 15 ms following light onset, which indicates that such activation *in vivo* should allow similar identification of pGABA neurons in mice.

Study of GABA neurons in TG anesthetized mice

The response of neurons was subsequently studied in the LDT/SubLDT of TG urethane-anesthetized (TG-A) mice (95 units in 6 mice) (Figs. 1, 4). All units were first tested with a short (5–15 ms) light pulse to determine their response. Of the units recorded, ~68% responded within the SLP by emitting a spike during the light pulse and were thus considered to be pGABA units (Fig. 4*A*). The units submitted to juxtacellular labeling included responding, pGABA units ($n = 59$ or ~91%) and some nonresponding, pNon-GABA units ($n = 6$ or 9%). Of the responding units, 18 were Nb-labeled, GAD- or GABA-immunopositive. Of the responding units that were Nb-labeled and immunostained for GABA ($n = 7$), 71% were GABA$^+$ ($n = 5$). As for the cell shown in Figure 2*B*, a major proportion (80%) of the Nb$^+$/GABA$^+$ cells among responding units also manifested intrinsic YFP in the plasma membrane confirming the expression of ChR2-EYFP in most of the responding Nb-labeled GABA neurons of the TG-A mice (Fig. 1*B*).

In the TG-A mice, the average latency to spike for the pGABA units during the SLP (≤15 ms) was 6.01 ± 0.37 ms (range 2.0-12.33 ms, $n = 63$; Table 2; Fig. 4*B*). However, the action potential was often preceded by an apparent brief hyperpolarization of the membrane (Fig. 4*A*), suggesting that pGABA units also received IPSPs from other locally activated pGABA units or their axons as observed *in vitro*. The average spike width during the light pulse was 1.18 ± 0.03 ms ($n = 59$) and not different from that during spontaneous spiking (1.12 ± 0.03 ms, $n = 53$; Table 2). With long (1-5 s) CLPs, the pGABA units fired continuously (Fig. 4*C*) with a moderately fast mean ADR (31.89 ± 3.03 Hz, $n = 59$), which included some higher frequency spiking (Fig. 4*D*) and yielded an overall mean IFF of ~42 Hz (41.86 ± 4.32 Hz, $n = 59$) (Table 2). Many pGABA units were also able to follow repetitive 10 ms light pulses fairly faithfully up to 50 Hz (Fig. 4*E*,*F*). All the pGABA units tested in the TG-A mice ($n = 48$) were found at 1 Hz photostimulation to have >90% fidelity; a significant proportion (35%), considered to have high fidelity, showed fidelity at 40 or 50 Hz of ≥75%; another proportion (40%), considered to have moderate fidelity, showed a decrement in fidelity at 20 Hz to ≥50%; and the remainder (25%), considered to have low fidelity, showed a decrement in fidelity at 10 Hz to ≥50%. During the CLP, units of these different groups fired at significantly different rates, with the high-fidelity group reaching a mean IFF of 85.36 ± 9.58 Hz, the moderate-fidelity group a mean IFF of 28.69 ± 2.35 Hz, and the low-fidelity group a mean IFF of 26.53 ± 5.50 Hz (ANOVA, $F = 29.93$, df = 2,41; $p < 0.001$, with HF group > MF and LF, $p < 0.05$ in *post hoc* paired comparisons with Bonferroni correction). Thus, although heterogeneous in firing properties, the pGABA units were generally relatively fast-firing and appeared to reach their highest rates of tonic firing during the CLP stimulation that was thus used across neurons in the study of their role in modulation of the EEG (below).

Although ~30% of units recorded in the LDT/SubLDT did not respond within the short (15 ms) light pulse ($n = 29$) and were thus considered to be pNon-GABA units, almost all of these units changed their ADR during a long (~5 s or longer) CLP by either increasing (28%) or decreasing (72%) their discharge rate (Fig. 5*A*,*B*). Being highly variable, the mean latency to spike during the CLP for the pNon-GABA units, which increased their discharge, was 86.89 ± 42.43 ms ($n = 6$). Concerning those units which decreased their discharge, they were almost all inhibited for the full duration of the CLP (Fig. 5*B*). Comparing groups, the spontaneous spike width of all pNon-GABA units (1.28 ± 0.09 ms, $n = 23$; Table 2) was on average larger than that of the pGABA units (1.12 ± 0.09 ms, $n = 53$; $t = 2.30$, df = 74, $p = 0.051$), although with considerable overlap. In addition to glutamatergic neurons (Boucetta et al., 2014), these pNon-GABA units would include cholinergic units, which have relatively broad spikes (1.60 ± 0.09 ms), as previously measured in pACh LDT/SubLDT neurons in TG mice (Cisse et al., 2018). In sum, the majority of the pNon-GABA units, which had on average broader spikes than the pGABA units, were inhibited with photic activation of the pGABA units.

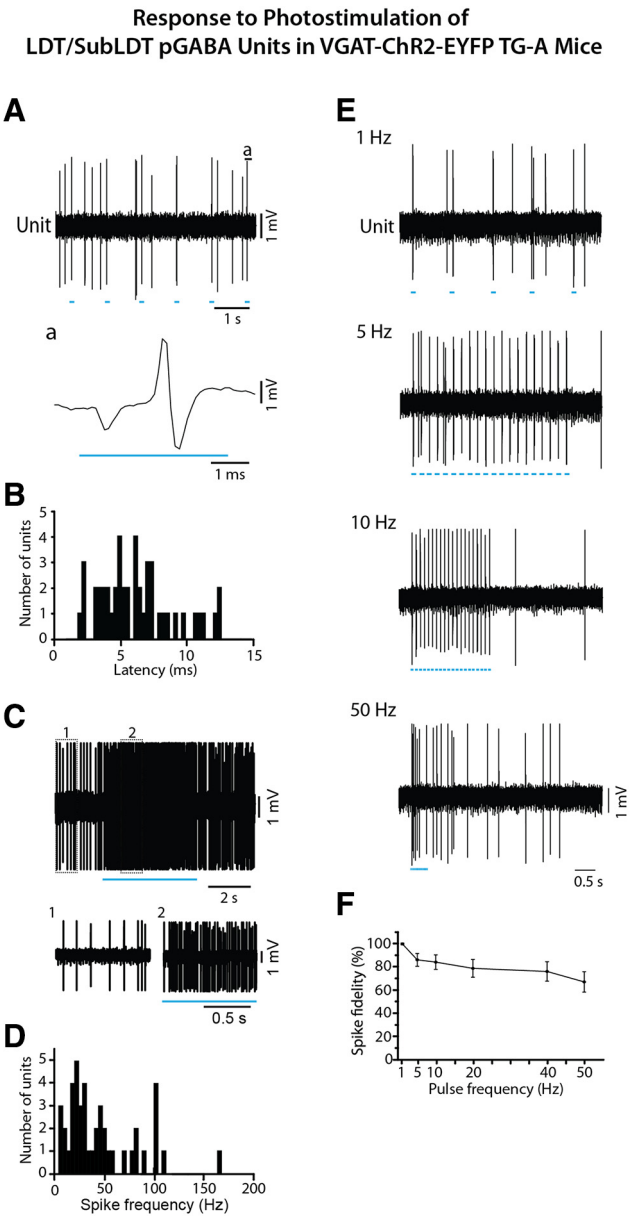

Figure 4. Response of LDT/SubLDT units to blue light stimulation *in vivo* in *VGAT-ChR2-EYFP TG* mice. pGABA units were studied in urethane-anesthetized mice. ***A***, *In vivo*, spiking in response to SLPs (~5 ms duration applied every second) by a pGABA unit in a TG-A mouse (unit #13 in Mouse VGAT77). Segment of trace a is expanded below and shows a brief hyperpolarization at ~1 ms preceding the spike at ~2 ms. ***B***, The spike latencies of units identified as pGABA ($n = 63$ units from 6 TG-A mice). ***C***, Response of pGABA unit (#13 inVGAT77) to a CLP (~5 s), expanded in 1 and 2 below. ***D***, The IFFs of pGABA units ($n = 58$) during long (1-5 s) CLPs when they fired repetitively. ***E***, Spiking of pGABA unit (#13 inVGAT77) in response to short (~10 ms) light pulses at different frequencies. ***F***, Spike fidelity of pGABA units ($n = 15$ from Mouse VGAT77) to SLPs at different frequencies (mean ± SEM).

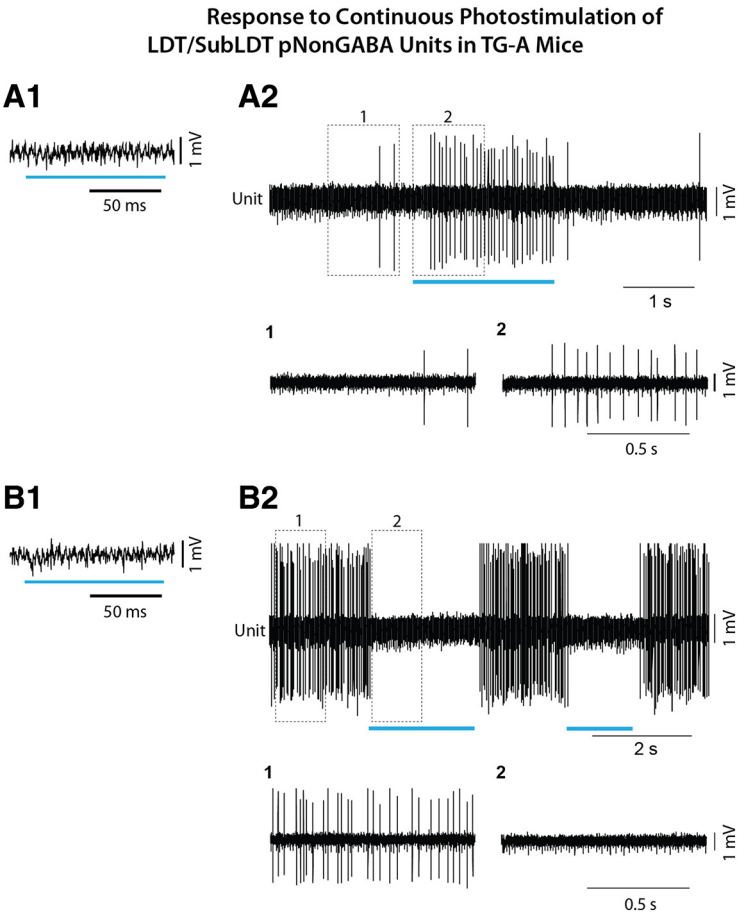

Figure 5. Response of LDT/SubLDT pNon-GABA units to long light pulses in TG-A mice. ***A***, Unit (#8 in Mouse VGAT77) identified as pNon-GABA by the failure to spike during SLPs (here ~100 ms, ***A1***) responded during a long (~2 s) CLP by a delayed increase in discharge, as illustrated in expanded segments (1, 2 below, ***A2***). ***B***, Another pNon-GABA unit (#7 in Mouse VGAT84) identified by the failure to spike during light pulses (here ~100 ms, ***B1***) ceased firing during a long (~2 s) CLP, as illustrated in expanded segments (1, 2 below, ***B2***).

In response to a long (1-5 s) CLP, the pGABA units increased their discharge before any changes in EEG activity, which were sometimes apparent by a decrease in the irregular slow activity and overall amplitude over the retrosplenial cortex in the TG-A mice (Fig. 6*A*,*B*). Across units, the average latency to the first spike was 3.88 ± 0.72 ms and that estimated for the change in EEG activity 236.44 ± 53.18 ms ($n = 9$). All pGABA units (48 of 48) increased their ADR, yielding a significant increase in mean ADR from 6.44 ± 1.30 Hz before to 34.53 ± 3.49 Hz during the CLP (paired *t*, $t = -9.68$, df = 47, $p < 0.001$; Table 3). The majority of units (44 of 48) fired at a higher IFF with a significant increase in the mean IFF from 18.92 ± 4.67 Hz before to 45.68 ± 5.10 Hz during the CLP (paired *t*, $t = -3.96$, df = 47, $p < 0.001$; Table 3) (Fig. 6*C-F*). Across units and mice, the changes in EEG activity were variable, showing decreases in δ activity in more than half ($n = 27$ of 52) but minimal change or small increases in other cases. Accordingly, there was no consistent or significant change in mean amplitude of δ activity (0.5-3.5 Hz) going from 14.33 ± 1.05 mV before to 13.87 ± 1.05 mV during the CLP (Table 3) or of γ activity (30-58 Hz) going from 4.81 ± 0.31 mV before to 5.09 ± 0.28 mV during the CLP ($n = 41$). In sum, although CLP stimulation elicited an increase in tonic firing rate of the pGABA units, it did not evoke a consistent change in slow or fast EEG activity in the TG-A mice.

Delivery of RLPs at a slow theta frequency (100 ms at 4 Hz for ~5 s), which was similar to the rhythmic slow activity (RSA) frequency evoked by somatosensory stimulation under urethane anesthesia (Cisse et al., 2018), resulted in high-frequency spiking during each light pulse by the pGABA units and a shift from irregular slow activity to RSA in the EEG of the TG-A mice (Fig. 7*A-C*). Their ADR increased in every unit (43 of 43) yielding a significant increase in the mean rate from 3.92 ± 0.84 Hz before to 22.35 ± 2.63 Hz during RLP stimulation (paired *t*, $t = -8.27$, df = 42, $p < 0.001$; Table 3). With the train of RLPs, the average latency to the first spike of the pGABA units was 6.80 ± 2.13 ms during the first pulse and that to the EEG change was 363.25 ± 57.26 ms ($n = 8$). The units fired during each light pulse and turned off at the end of each pulse, although they often resumed firing before subsequent pulses. Most units ($n = 41$ of 43) fired phasically during the RLPs, some with a primary mode IFF in the very high-frequency range (>80 Hz, $n = 16$), others in a high-frequency range (30-80 Hz, $n = 20$) or moderate-frequency range (16-29 Hz, $n = 5$) (Table 4), which was considered as phasic burst or cluster firing during the RLPs. In comparing the primary mode IFF in the same units before and during the RLPs, a shift from predominantly slow tonic spiking to high-frequency phasic spiking was evident (Pearson's $\chi^2 = 12.57$, df = 6, $p = 0.050$; Table 4). Most units manifested at least two modes of firing (41 of 43 units), with one mode at a moderate to very high (>15 Hz) frequency range (20-500 spikes/s) and one mode in a slow frequency range (<16 Hz), which reflected rhythmic phasic firing around the slow theta rhythm. Comparing the IFFs, there was a significant increase between the mean primary mode firing before the RLPs (31.12 ± 7.91 Hz) and the mean high-frequency mode firing (>15 Hz) during the RLP stimulation (127.33 ± 23.96 Hz, paired *t*, $t = -3.65$, df = 26, $p = 0.001$; Table 3). The mean low-frequency mode (0.5-15 Hz) during the RLPs was 5.83 ± 0.25 Hz ($n = 23$; Table 3). Most units showed rhythmic spiking at ~4 Hz in the autocorrelation histogram (ACH) during the RLPs (38 of 43 cases; Table 4; Fig. 7*E*). The EEG was driven to a primary peak frequency of ~4 Hz with many units (20 of 43; Table 4) or showed a secondary peak at ~4 Hz (7 of 43 units) (Fig. 7*C*). A majority of units showed cross-correlated activity with the EEG at this frequency in the STA ($n = 31$ of 43 units; Table 4; Fig. 7*C–F*). These changes were not associated with consistent changes in mean EEG δ activity (0.5-3.5 Hz), which was on average 13.60 ± 0.90 mV before and 14.58 ± 0.92 mV during RLP stimulation ($n = 43$; Table 3), or in mean γ activity (30–58 Hz), which was 4.88 ± 0.26 mV before and 4.93 ± 0.18 mV during RLP stimulation ($n = 43$). In sum, RLP stimulation at a low theta frequency (~4 Hz) in the TG-A mice evoked rhythmic phasic burst or cluster firing at a low theta rhythm by the

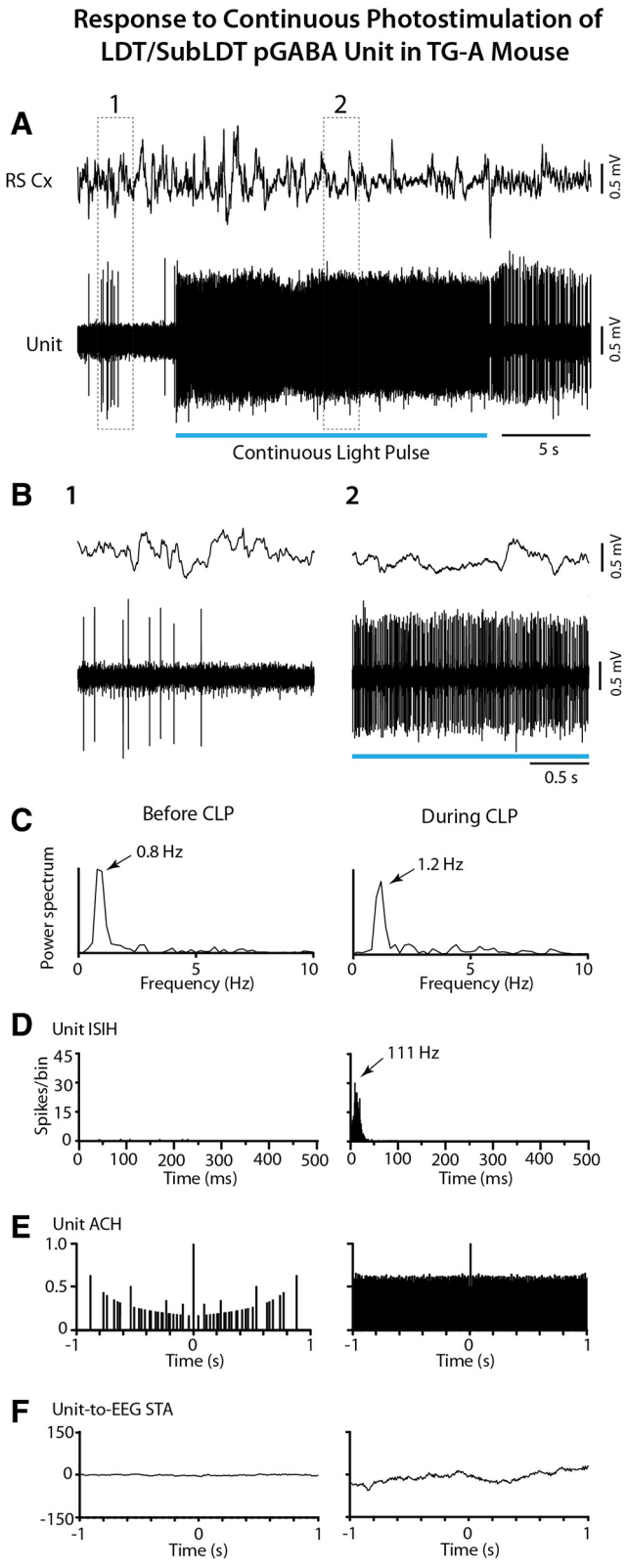

Figure 6. Response of LDT/SubLDT pGABA unit along with EEG to CLP stimulation in TG-A mouse (unit #2 in Mouse VGAT77). ***A***, A long (~20 s) CLP was delivered during EEG irregular slow activity and elicited an immediate and continuous increase in spiking of the unit, which was associated with a progressive change in EEG activity. ***B***, Shown in segments expanded from before (1) and during (2) the CLP, the unit increased its discharge to very high-frequency spiking, whereas the EEG showed a gradual reduction in slow wave activity and greater predominance of higher frequency activity. ***C***, As evident in the power spectra, there was a slight shift in the low-frequency peak. ***D***, The unit ISI histogram (ISIH) revealed high pGABA neurons that was associated with low theta or RSA on the EEG of limbic cortex.

CLPs and RLPs were also tested in TG-A mice on pNon-GABA units, which did not respond with a short latency to the SLPs. In those cells that were inhibited by the CLPs (above, Fig. 5*B*), RLPs also stimulated rhythmic discharge, as in the pGABA units, however, by firing during the off phase of the light pulses (Fig. 8*A*,*B*). Among pNon-GABA units, the average IFF of the units was 19.91 ± 4.72 Hz ($n = 5$) before and varied during the RLPs. Most pNon-GABA units showed, like the pGABA units, two or more modes of instantaneous firing frequencies with a primary mode in the high-frequency range (>15 Hz; mean of 54.19 ± 9.91 Hz, $n = 10$), including 16-29 Hz (2 of 10 units), 30-80 Hz (4 of 10 units), or >80 Hz (2 of 10 units) (Table 4), which reflected cluster or burst firing at a theta frequency. All units showed a low-frequency range mode (<16 Hz) near the theta frequency with a mean IFF of 5.42 ± 0.28 Hz ($n = 10$) (Fig. 8*D*). In the majority of units, there was evidence of rhythmic firing in the ACH at ~4 Hz (6 of 10 units) and participation in the rhythmic EEG in the STA at this frequency (7 of 10 units; Table 4; Fig. 8*C*–*F*). In sum, pNon-GABA units were also driven in a reciprocal manner to fire phasically with RLPs in association with RSA or low theta on the EEG of TG-A mice.

Study of GABA neurons in TG unanesthetized (TG-UA) mice

The response and properties of neurons in the LDT/SubLDT were subsequently studied in head-fixed TG-UA mice ($n = 49$ cells in 9 mice) (Fig. 1*A*,*B*). Of the units selected for juxtacellular labeling ($n = 19$) in TG-UA mice, approximately half responded to the SLP and were thus considered pGABA neurons ($n = 9$ or ~47%) and the others, which did not respond, pNon-GABA neurons ($n = 10$ or ~53%). Of the juxta-submitted units, all were successfully labeled with Nb in the LDT/SubLDT or surrounding area. From the juxta-submitted responding or pGABA units, 67% of Nb-labeled cells were identified as $Nb^+/GABA^+$ and of these, 63% were identified as $Nb^+/GABA^+/EYFP^+$ (Figs. 1*B*, 2*C*,*D*).

The pGABA units in the LDT/SubLDT of TG-UA mice showed short spike latencies during the (≤15 ms) SLP with a mean latency of 5.99 ± 0.67 ms (range 1.33-13.00 ms, $n = 23$; Table 2). The average spike width of the pGABA units was 1.10 ± 0.07 ms ($n = 8$) during the light pulse and did not differ significantly from that during spontaneous activity (1.19 ± 0.08 ms, $n = 21$; Table 2). With a long (1-5 s) CLP, the pGABA units fired at the onset but not necessarily for the full duration of the light pulse. Across units, the average discharge during the CLP was 62.52 ± 29.11 Hz ($n = 8$; Table 2). The spiking was variable from irregular slow tonic to high frequency (30-80 Hz) to burst-like (>80 Hz), yielding an average IFF of 116.32 ± 41.74 Hz across units ($n = 8$; Table 2). Given that the photostimulation often elicited behavioral and EEG arousal responses to the light pulses in the

←

IFFs (the reciprocal of the interval values) with a mode (indicated by arrow) at 111 Hz during the CLP. ***E***, In the ACH, the unit showed no rhythmicity in its spiking. ***F***, In the Unit-to-EEG STAs (with mV on vertical axis), there was no evidence of rhythmic or cross-correlated activity before or during periods of analysis corresponding to the ~5 s periods from EEG and unit activities illustrated.

Table 3. Mean values of unit ADR and IFF with EEG δ amplitude measures in TG-a and TG-UA mice before and during CLP or RLP stimulation and in WT-UA mice during SWS, PS, and aW[a]

Group	Stimulation	Unit activity Unit ADR (Hz)			Unit firing Unit IFF primary mode (Hz)				EEG activity δ Amplitude (mV)		
TG-A		Before	During	*t*	Before	During	*t*	During	Before	During	*t*
	CLP[b]	6.44 ± 1.30	34.53 ± 3.49	***	18.92 ± 4.67	45.68 ± 5.10	***		14.33 ± 1.05	13.87 ± 1.05	
		n = 48	*n* = 48		*n* = 48	*n* = 48			*n* = 41	*n* = 41	
						(HF mode)		(LF mode)			
	RLP[c]	3.92 ± 0.84	22.35 ± 2.63	***	31.12 ± 7.91	127.33 ± 23.96	***	5.83 ± 0.25	13.60 ± 0.90	14.58 ± 0.92	
		n = 43	*n* = 43		*n* = 27	*n* = 27		*n* = 23	*n* = 43	*n* = 43	
TG-UA		Before	During	*t*	Before	During	*t*	During	Before	During	*t*
	CLP[d]	18.09 ± 7.07	62.52 ± 29.11		72.69 ± 33.22	121.04 ± 41.74			8.45 ± 1.14	5.82 ± 0.40	*
		n = 7	*n* = 7		*n* = 7	*n* = 7			*n* = 6	*n* = 6	
						(HF mode)		(LF mode)			
	RLP[e]	17.21 ± 6.67	32.69 ± 7.13	***	32.76 ± 11.35	129.22 ± 54.33		9.59 ± 1.07	15.11 ± 1.18	10.73 ± 1.45	*
		n = 9	*n* = 9		*n* = 8	*n* = 8		*n* = 6	*n* = 8	*n* = 8	
WT-UA	None	SWS	PS	*t*	SWS	PS	*t*	PS (LF mode)	SWS	PS	*t*
		4.20 ± 2.55	13.76 ± 1.17	*	10.67 ± 6.99 Hz	108.00 ± 7.18	**	7.23 ± 0.39	16.19 ± 3.36	4.85 ± 0.55	*
		n = 5	*n* = 5		*n* = 5	*n* = 5		*n* = 5	*n* = 5	*n* = 5	
			aW			aW	*			aW	
			11.48 ± 3.01			87.40 ± 19.40				5.29 ± 0.17	*
			n = 5			*n* = 5				*n* = 5	

[a]Data are mean ± SEM for number of units indicated and compared by paired *t* tests between the following: before and during photostimulation or between PS and SWS or aW and SWS for sleep-wake states.
[b]CLP of ~5 s.
[c]RLPs of 100 ms at 4 Hz for ~5 s.
[d]CLP of ~1-5 s.
[e] RLPs of 50 ms at 8 Hz for ~5 s.*$p \leq 0.05$; **$p \leq 0.01$; ***$p \leq 0.001$; Bonferroni corrections for *post hoc* multiple comparisons.

unanesthetized mice (see below), it was not possible to administer repetitive 10 ms light pulses to test for spike fidelity, as was done in the anesthetized mice, even with considerable reduction of the light intensity (see Materials and Methods). It was also noticed that it was much more difficult to reliably drive the unit activity by photostimulation in the TG-UA mice compared with the TG-A mice, since there was considerably more spontaneous activity.

All the recorded units, which did not respond during a short (≤15 ms) light pulse and were thus considered pNon-GABA units in the LDT/SubLDT ($n = 20$) of the TG-UA mice, nonetheless changed their discharge rate during a long (~1-5 s) CLP, as seen in the TG-A mice. Half increased and half decreased their rate of discharge (not shown). The average latency to spike during the long light pulse for the pNon-GABA units, which increased their rate, was 159.17 ± 66.89 ms ($n = 6$). For those that decreased their rate, they were almost all inhibited for the full duration of the CLP (1-5 s), as in the TG-A mice (above, Fig. 5*B*). The average spike width of all pNon-GABA units in the TG-UA mice was 1.42 ± 0.16 ms ($n = 20$), ostensibly, but not significantly, larger than that of the pGABA units (1.19 ± 0.08 ms, $n = 21$; with *t* test, $t = 1.32$, df = 39, $p = 0.195$) due to considerable overlap.

To examine the response of pGABA LDT/SubLDT neurons in relation to changes in EEG activity in the TG-UA mice, a long (1-5 s) CLP was delivered. When possible, the photostimulation was delivered when the EEG manifested irregular slow wave activity typical of slow wave sleep (SWS); however, in the UA mice and particularly in association with delivery of test light pulses, high-amplitude slow wave activity was often not present. The test periods of photostimulation were thus often taken from periods of lower-amplitude slow waves more typical of the transition to SWS or occasionally even quiet W (Del Cid-Pellitero et al., 2017). Indeed, the CLPs were often stopped by the experimenter at 1-2 s or maximum 4 s due to provocation of arousals and consequent loss of unit recording in the TG-UA mice. The unit activity and EEG were thus much more variable in the TG-UA mice compared with the TG-A mice. The pGABA units in the LDT/SubLDT generally increased their rate of discharge during the CLP, whereas the EEG appeared to be reduced in amplitude (Fig. 9), although the duration of the increased spiking and the shift in EEG activity were variable across cases. The mice often showed movements of the vibrissae and muzzle with evidence of arousal by the end or with the termination of the CLP. For the pGABA units tested, the latency to spike during the long CLP was in some cases much longer than that recorded during the SLP, yielding a mean of 22.60 ± 12.10 ms ($n = 5$). A shift in EEG activity was apparent in some of these recordings having a mean latency of 175.75 ± 94.52 ms ($n = 4$). All units increased their ADR ($n = 8$ of 8), such that their mean rate increased from 18.09 ± 7.07 Hz before to 62.52 ± 29.11 Hz during the CLP, however not significant given the variability in rates across units (with paired *t*, $t = -1.48$, df = 7, $p = 0.181$; Table 3). The mean IFF increased variably ($n = 3$ of 5) from a mean of 72.69 ± 33.22 Hz before to 121.04 ± 41.74 Hz during the CLP (with paired *t*, $t = -1.29$, df = 6, $p = 0.245$; Table 3). The increases in IFF reflected moderate to more commonly high-frequency spiking (30-80 Hz) and very high-frequency spiking (>80 Hz) during the light pulse. There was a decrease in δ amplitude (0.5 Hz-4.0 Hz) in all cases (6 of 6), with a significant decrease in the mean amplitude from 8.45 ± 1.14 mV before to 5.82 ± 0.40 mV during the CLP (paired *t*, $t = 2.65$, df = 5, $p = 0.045$; Table 3). γ band activity (30-58 Hz) also decreased in most cases (5 of 6) with an overall mean of 5.44 ± 0.23 mV before and 4.40 ± 0.26 mV during the CLP (paired *t*, $t = 2.65$, df = 5, $p = 0.045$). In sum, in the TG-UA mice, CLP stimulation elicited high-frequency spiking in the pGABA neurons, which was associated with behavioral arousal and a decrease in δ EEG activity, although not with a reciprocal increase in γ EEG activity, which normally accompanies arousal.

The effects of delivering RLPs at a high theta frequency (50 ms at 8 Hz for 1-5 s), like that of active/attentive (a) W or PS,

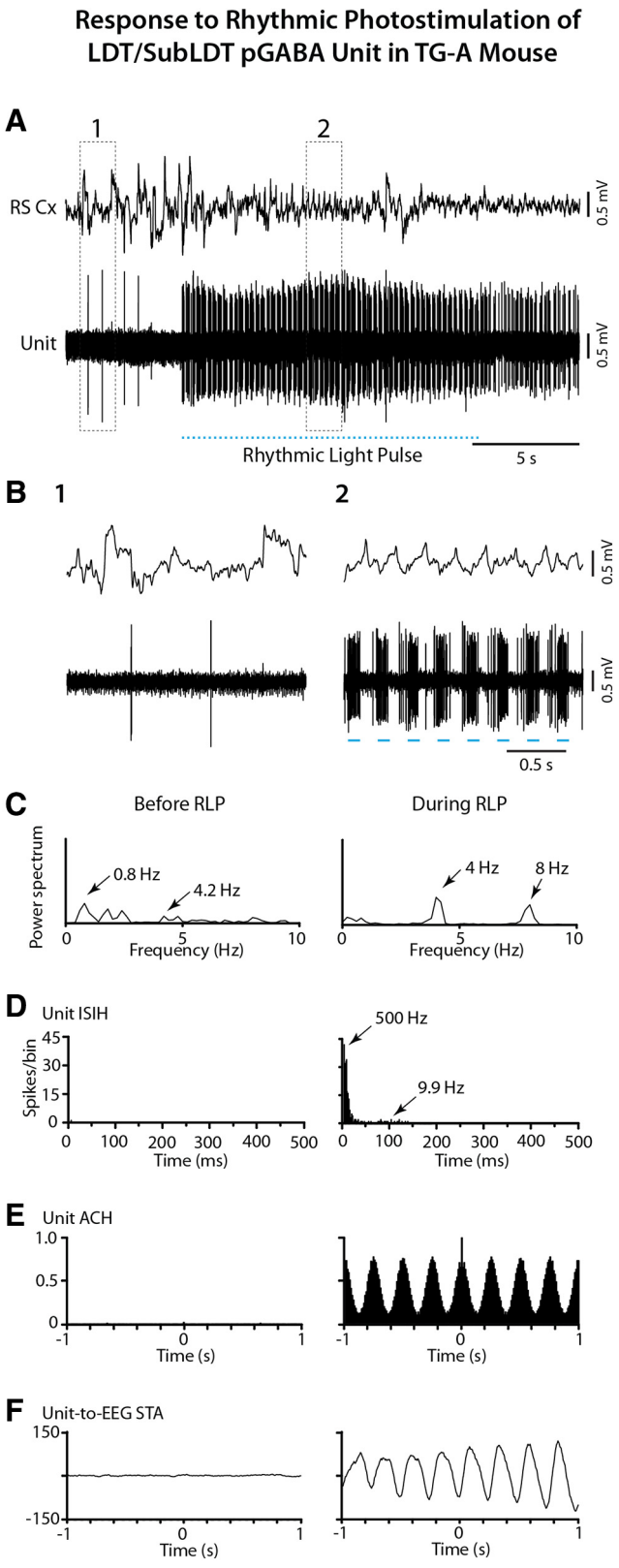

Figure 7. Response of LDT/SubLDT pGABA unit along with EEG to RLP stimulation in a TG-A mouse (#2 in Mouse VGAT77, as shown in Fig. 6). ***A***, A series of RLPs (100 ms at 4 Hz for ~10 s) were delivered during a period of EEG irregular slow activity and elicited rhythmic phasic spiking of the unit along with EEG RSA. ***B***, As shown in the expanded traces 1 and 2, the pGABA unit was driven by the light pulses to fire in high-frequency trains or bursts of spikes, whereas the EEG was progressively driven into RSA. ***C***, Evident in the power spectra, the EEG shifted from irregular slow activity (~0.8 Hz) before the RLPs to RSA at 4 Hz with a harmonic at 8 Hz during RLPs. ***D***, In the ISIH, the unit firing occurred in high-frequency bursts during the RLPs (primary mode at 500 Hz) with a recurrence at slower frequencies (arrow in middle of broad low-frequency mode). ***E***, In the ACH, the unit firing showed rhythmicity at ~4 Hz. ***F***, In the Unit-to-EEG STA, unit activity was cross-correlated with the EEG RSA at 4 Hz. For graph details and abbreviations, see legend to Figure 6.

was subsequently examined on the activity of the pGABA LDT/SubLDT units and the concomitant EEG activity in the head-fixed TG-UA mice. As seen with the long CLP, there was an increase in unit discharge and coextensive change in EEG activity (Fig. 10*A*,*B*). Movements of the whiskers and muzzle were often evident in the video recordings with apparent arousal by the end or with the termination of the RLP stimulation. The units tended to spike with each 50 ms pulse and to cease firing at the end of each pulse, yet they sometimes spiked just before the next pulse and/or failed to spike with successive pulses in the train. All units increased their average rate of discharge (8 of 8), yielding a significant increase in the mean ADR from 17.21 ± 6.67 Hz before to 32.69 ± 7.13 Hz during the RLPs (paired *t*, $t = -5.09$, df = 8, $p = 0.001$; Table 3). All units fired phasically (8 of 8) at either a very high-frequency bursting mode (>80 Hz, $n = 3$) or a high-frequency cluster mode (30-80 Hz, $n = 5$; Table 4). Comparing the mean primary firing mode before stimulation to the high-frequency (>15 Hz) mode during RLP stimulation, almost all neurons manifested an increase in IFF (7 of 8) that was associated with a trend of an increase in the mean firing from 32.76 ± 11.35 Hz before to 129.22 ± 54.33 Hz during the RLPs (range 42-500 spikes/s; paired *t*, $t = -2.07$, df = 7, $p = 0.078$; Table 3). Most units also manifested a low-frequency mode near the theta frequency of the stimulation ~8 Hz (9.59 ± 1.07 Hz, $n = 6$; Table 3), indicating rhythmic phasic firing driven by the RLPs at ~8 Hz. Half the pGABA units manifested rhythmic firing at ~8 Hz (4 of 8), which was cross-correlated with the high theta EEG activity at ~8 Hz in some cases (2 of 8 units; Table 4) (Fig. 10*C*-*F*). δ amplitude (0.5-4.0 Hz) was decreased in most cases (8 of 9), resulting in a significant decrease across cases from a mean of 15.11 ± 1.18 mV before to 10.73 ± 1.45 mV during the RLPs (paired *t*, $t = 2.44$, df = 7, $p = 0.045$; Table 3). As an index of theta activity, the ratio of high theta (6.0-10.0 Hz) over δ (0.5-4 Hz) was significantly increased with means of 1.12 ± 0.14 before and 2.09 ± 0.36 during the RLPs (paired *t*, $t = -2.44$, df = 8, $p = 0.041$). γ amplitude did not show significant changes with means of 3.54 ± 0.78 mV before and 3.90 ± 0.91 mV during the RLPs (paired *t*, $t = -0.92$, df = 6, $p = 0.396$). In sum, RLP stimulation in the TG-UA mice evoked rhythmic firing in a burst or cluster mode of spiking often around a high theta frequency (~8 Hz), which was associated with high theta EEG activity on the limbic cortex.

CLPs and RLPs were also tested in the TG-UA mice on some pNon-GABA units that did not respond with a short latency to the SLPs. In some cells, which were inhibited by the CLP, RLPs stimulated rhythmic discharge, as in the pGABA units, however, by firing during the off phase of the light stimulation (Fig. 11), when the pGABA units were silent. The average IFF of the pNon-GABA units was 32.50 ± 15.92 Hz ($n = 5$) before the RLP stimulation. Many fired phasically during the RLPs (4 of 5), 1 unit at very high frequency (>80 Hz) and 3 in a high-frequency range of 30-80 Hz (Table 4), yielding a mean IFF in the high-frequency range of 71.64 ± 10.20 ($n = 4$). In some units, there was evidence of rhythmic firing of the unit in the ACH at ~8 Hz (2 of 5 units) and participation in the rhythmic EEG at this frequency in the STA (3 of 5 units; Table 4; Fig. 11*C*–*F*). There was

Table 4. Number of pGABA and pNon-GABA units manifesting different primary modes of firing frequencies, rhythmic firing (ACH), and cross-correlated firing (STA) with the EEG (PF) at low (4 Hz) or high (8 Hz) theta rhythms during RLP stimulation in TG-a and TG-UA mice or during natural sleep-wake states in WT-UA mice[a]

Group	Units	Stimulation	Unit IFF primary mode				Unit ACH F	EEG PF	STA F
TG-A				Before	During	During	During	During	During
	pGABA	RLP	1-15 Hz	11	0	2	~4 Hz: 38	20	31
			16-29 Hz	6	3	5			
			30-80 Hz	8	10	20			
			>80 Hz	2	14	16			
			Total	$n = 27$	$n = 27$	$n = 43$	$n = 43$	$n = 43$	$n = 43$
	pNon-GABA	RLP	1-15 Hz	1	1	2	~4 Hz: 6	5	7
			16-29 Hz	2	0	2			
			30-80 Hz	1	3	4			
			>80 Hz	0	0	2			
			Total	$n = 4$	$n = 4$	$n = 10$	$n = 10$	$n = 10$	$n = 10$
TG-UA				Before	During		During	During	During
	pGABA	RLP	1-15 Hz	4	0		~8 Hz: 4	6	2
			16-29 Hz	1	0				
			30-80 Hz	2	5				
			>80 Hz	1	3				
			Total	$n = 8$	$n = 8$		$n = 8$	$n = 8$	$n = 8$
	pNon-GABA	RLP	1-15 Hz	3	1		~8 Hz: 2	3	3
			16-29 Hz	0	0				
			30-80 Hz	2	3				
			>80 Hz	0	1				
			Total	$n = 5$	$n = 5$		$n = 5$	$n = 5$	$n = 5$
WT-UA				SWS	PS		PS	PS	PS
	GABA	None	1-15 Hz	4	0		~8-9 Hz: 1	5	0
			16-29 Hz	0	0				
			30-80 Hz	1	0				
			>80 Hz	0	5				
			Total	$n = 5$	$n = 5$		$n = 5$	$n = 5$	$n = 5$

[a]Number of units manifesting different primary mode IFFs and slow rhythmic discharge at a low or high theta rhythm in the ACH and the STA to indicate cross-correlated rhythmic firing with the EEG at its theta peak frequency (PF).

a significant increase in the ratio of high theta (6.0-10.0 Hz) over δ (0.5-4 Hz) EEG, which reflects theta activity, from 1.12 ± 0.16 to 2.45 ± 0.38 (paired t, $t = -2.73$, df = 5, $p = 0.041$). In sum, the pNon-GABA units were driven to fire in phasic bursts or clusters of spikes around a high theta frequency (~8 Hz) in a reciprocal manner to the pGABA neurons presumably by rebound from inhibition during the RLPs.

For control, both CLPs and RLPs were tested in WT-UA mice to determine whether any changes in unit or EEG activity would occur with the light stimulation. In units that were selected for their similarity to those identified as pGABA units (above) and of which a proportion were juxta-submitted, Nb-labeled, and identified as $GABA^+$ (below), their spike width was similar to that of the pGABA units (1.02 ± 0.09 ms, $n = 11$; Table 2). These units in the WT mice did not show changes in their ADR before versus during CLPs (9.84 ± 6.75 vs 7.34 ± 5.97 Hz, $n = 4$), and the EEG showed no significant changes. The units also did not show changes in their ADR before versus during RLPs (22.49 ± 12.45 vs 14.15 ± 3.35 Hz, $n = 8$). Neither the units nor the EEG in the WT mice showed rhythmic activity at 8 Hz during the RLPs, and the ratio of high theta over δ EEG activity, which was significantly increased in the TG mice, was not different before versus during RLPs in the WT mice (1.22 ± 0.16 vs 1.10 ± 0.09, $n = 8$).

Study of GABA neurons in naturally sleeping-waking WT-UA mice

Neurons were recorded in the LDT/SubLDT of 3 WT-UA head-fixed mice during natural sleeping-waking and submitted to juxtacellular labeling with Nb for subsequent identification as GABA neurons. Being selected according to the characteristics of the pGABA units of the TG mice, 5 units were successfully recorded across the three states of W, SWS, and PS and were among Nb-labeled neurons which were located in the LDT/SubLDT and positively immunostained for GABA (Fig. 2*E*). These units had an average spike width of 1.03 ± 0.17 ms ($n = 5$). As evident in one unit, which was among Nb-labeled $GABA^+$ units (Fig. 12*A*,*B*), these units discharged at their highest average rates during aW (11.48 ± 3.01 Hz) and PS (13.76 ± 1.17 Hz) and could either be silent or fire at low rates during SWS (4.20 ± 2.55 Hz) (with repeated-measures ANOVA, $F = 5.51$, df = 2,8, $p = 0.031$; Table 3). They would accordingly fit the profile of W/PS-max active neurons (Boucetta et al., 2014). The different rates of GABA unit discharge were inversely associated with different amplitudes of δ activity (0.5-4.0 Hz) across the three states, being higher during SWS (16.19 ± 3.36 mV) than during aW (5.29 ± 1.17 mV) and PS (4.85 ± 0.55 mV) (with repeated-measures ANOVA, $F = 16.98$, df = 2,8, $p = 0.011$; Table 3). The ratio of high theta (6.0-10.0 Hz) over δ was higher during aW (1.82 ± 0.33) and PS (2.13 ± 0.35) than during SWS (0.87 ± 0.18) (with repeated-measures ANOVA, $F = 7.37$, df = 2,8, $p = 0.015$), whereas γ activity (30-58 Hz) was variably higher during aW (11.73 ± 1.35 mV) and PS (11.65 ± 2.43 mV) than during SWS (10.00 ± 0.94 mV) (with repeated-measures ANOVA, $F = 1.07$, df = 2,8, $p = 0.372$). All units displayed a different pattern of firing with much higher frequency (>80 Hz) and tendency to burst during aW and more so during PS than during SWS (Table 4), with the instantaneous firing frequencies during aW (87.40 ± 19.40 Hz) and PS

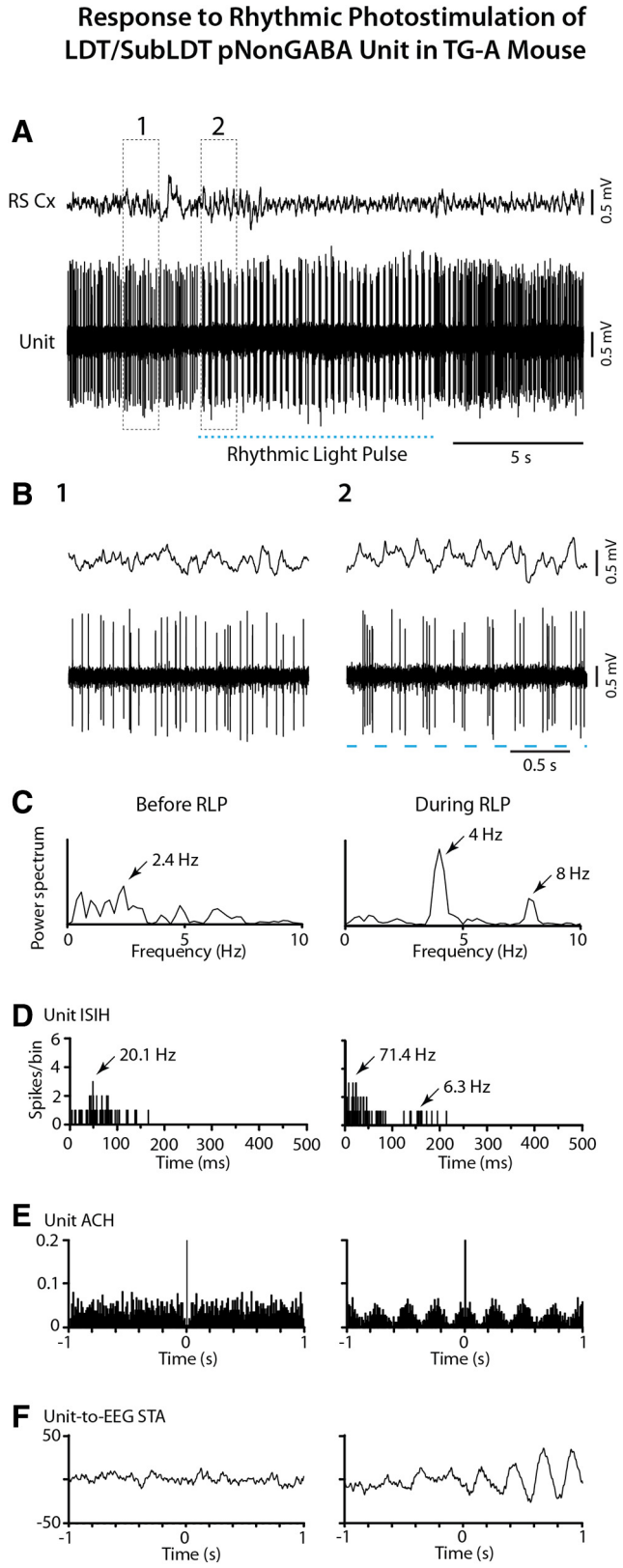

Figure 8. Response of LDT/SubLDT pNon-GABA unit along with EEG to RLP stimulation in a TG-A mouse (#3 in Mouse VGAT77). ***A***, A series of RLPs (100 ms at 4 Hz for ~8 s) was delivered during a period of EEG irregular activity and elicited rhythmic phasic spiking of the unit along with EEG RSA. ***B***, As shown in the expanded traces 1 and 2, the pNon-GABA unit was inhibited by the light pulses and thereby driven to fire phasically during the off period of the RLP stimulation, whereas the EEG was driven into RSA. ***C***, Evident in the power spectra, the EEG shifted from irregular activity before the RLPs to RSA at 4 Hz with a harmonic at 8 Hz during the RLPs. ***D***, In the ISIH, the unit firing in high-frequency spike trains during the off phase of the RLPs was evident (with a mode at 71 Hz) along with a secondary low-frequency mode near the RSA frequency. ***E***, In the ACH, the unit firing showed some rhythmicity at ~4 Hz. ***F***, In the Unit-to-EEG STA, the unit activity was very minimally cross-correlated with the EEG RSA at 4 Hz. For graph details and abbreviations, see legend to Figure 6.

(108.00 ± 7.18 Hz, range 90-125 spikes/s) being much higher than those during SWS (10.67 ± 6.99 Hz) (with repeated-measures ANOVA, $F = 21.27$, df = 2,8, $p = 0.005$; Table 3). The bursts consisted most commonly of 2 or 3 spikes. During PS, all units manifested one or more high-frequency modes (Table 4) and one low-frequency (<15 Hz) mode, which was in a high theta range (6-10 Hz) with a mean IFF of 7.23 ± 0.39 ($n = 5$; Table 3). The bursting during PS occurred in association with high theta EEG activity (~8-9 Hz) but generally showed weak rhythmicity (Fig. 12*C-F*), with clear rhythmicity in the ACH in only 1 of 5 units and no clear cross-correlation with the EEG theta activity in the STA (Table 4). The rhythmic bursting that did occur by the units was not continuous but episodic in contrast to limbic theta activity. In sum, the pGABA units fired phasically in clusters or bursts of spikes periodically during aW and especially PS in association with high theta EEG activity, although with relatively low rhythmicity or EEG cross-correlated activity.

Discussion

From *in vitro* and *in vivo* optogenetic study, the GABA neurons in the LDT/SubLDT region were found to be fast-firing neurons with the capacity to burst. With theta photostimulation, they fired in high-frequency spike clusters or bursts and could drive EEG theta activity in limbic cortex. High-frequency bursting by the GABA neurons was also found to occur naturally, though intermittently, during active/aW and PS in association with EEG theta activity.

Application of optogenetics in *VGAT-ChR2-EYFP TG* mice

We used *VGAT-ChR2-EYFP TG* mice to allow juxtacellular recording in association with photostimulation of the GABA neurons in the LDT/SubLDT, as we had previously done with *ChAT-ChR2-EYFP* mice for the ACh neurons (Cisse et al., 2018). According to the first application of such cell type-specific TG mice, they should provide relatively specific tagging of GABA and ACh cell types for optogenetics (Zhao et al., 2011). With the *VGAT-ChR2-EYFP* mice in that study, >85% of $GAD67^+$ cells were $EYFP^+$ and >85% of $EYFP^+$ cells were $GAD67^+$ in cortex and hippocampus; 100% of GAD^+ Purkinje cells were $EYFP^+$, and 100% of the $EYFP^+$ cells were GAD^+. Here, we also found that all Purkinje cells appeared to be $EYFP^+$ and $GAD67^+$. However, in the LDT/SubLDT, the GABA soma are very small, and with the EYFP being apparent only in the plasma membrane, the YFP staining was difficult to discern. We could thus neither use the YFP fluorescence to identify cells *in vitro* for recording, nor to assess the expression of ChR2-EYFP across GABA neurons in the LDT/SubLDT region. On the other hand, such selective labeling of the plasma membrane with ChR2-EYFP in the Tg mice can actually be considered positive, since the ChR2 should be transported to the membrane, where it functions as an ion channel (Nagel et al., 2003), whereas labeling through the cytoplasm suggests overloading of the cell with ChR2-EYFP, which can occur with viral transcription and have

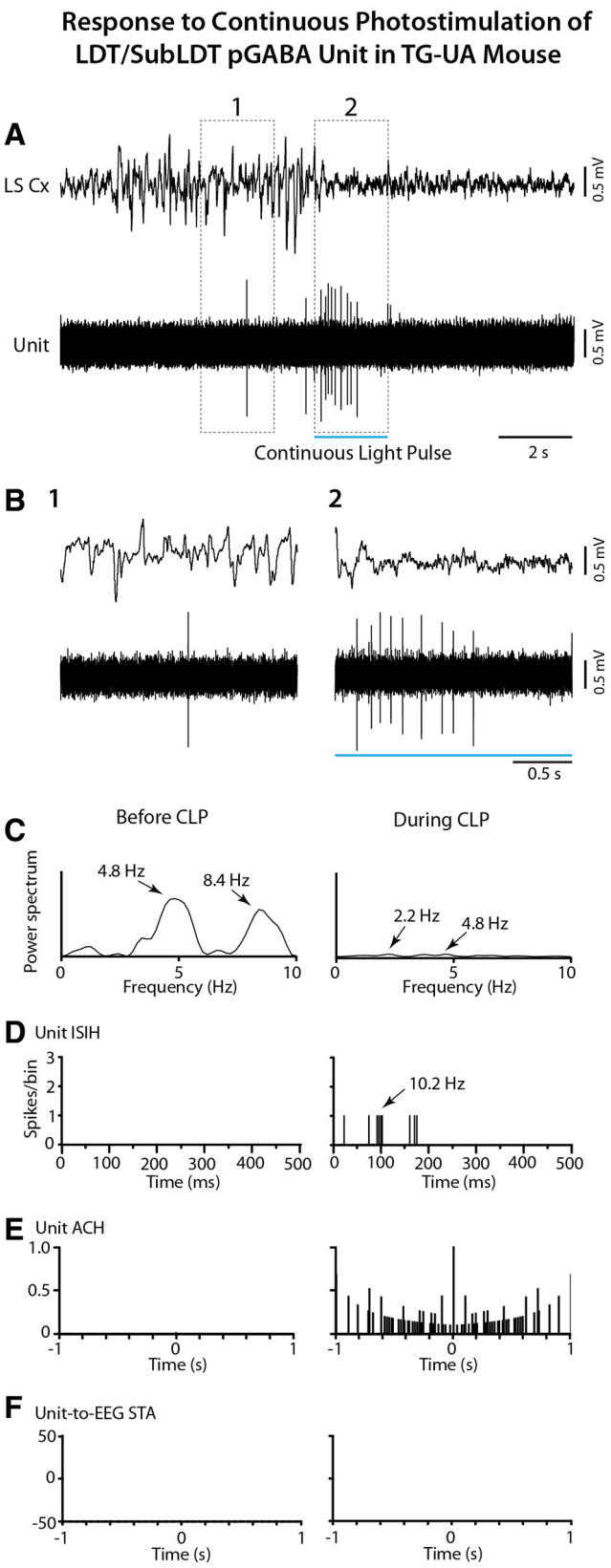

Figure 9. Response of LDT/SubLDT pGABA unit to CLP stimulation in a TG-UA mouse (#5 in Mouse CVGAT18). ***A***, A long (~2 s) CLP was delivered during EEG irregular activity and elicited an increase in spiking of the unit at the onset of the CLP, which was associated with a rapid change in EEG activity. ***B***, Shown in segments expanded from before (1) and during (2) the CLP, the unit increased its discharge to low-frequency tonic spiking, whereas the EEG showed a reduction in slow activity and greater predominance of low amplitude faster activity. ***C***, As evident in the power spectra, there was an overall reduction in slower EEG activity. ***D***, As evident in the ISIH, the unit fired at a relatively low frequency. ***E***, In the ACH, the unit showed no rhythmicity in its spiking. ***F***, In the Unit-to-EEG STA, there was no evidence of rhythmic or cross-correlated activity. For graph details and abbreviations, see legend to Figure 6.

deleterious effects on neurons and their physiology (Kalmbach et al., 2012; Ganini et al., 2017). Here, we assessed the presence of ChR2-EYFP in the recorded Nb-labeled cells and estimated that among the photo-responding neurons, ~70% of Nb-labeled GABA-immunopositive neurons were $EYFP^+$, and ~90% of Nb-labeled $EYFP^+$ neurons were GABA-immunopositive. However, given the possibility of false-negative immunostaining for GABA, the degree of eutopic expression of ChR2-EYFP may be higher than that estimated. Indeed, with photostimulation in the slice, we observed only IPSCs and never EPSCs that would have indicated activation of excitatory glutamate or ACh neurons, which lie intermingled with the GABA neurons (Wang and Morales, 2009). We nonetheless must remain cautious and assume that a minor proportion of the pGABA neurons could be Non-GABA neurons.

Properties of the GABA and Non-GABA neurons in *VGAT-ChR2-EYFP TG* mice

In brain slices, the vast majority of pGABA neurons in the LDT manifested the capacity to transiently discharge at high frequencies and sustain moderate rates of firing but also to discharge with low-threshold spike bursts from hyperpolarized membrane potentials, as typical of previously described Type I LDT neurons (Leonard and Llinas, 1990; Kamondi et al., 1992). Such bursts were also evident *in vivo* in anesthetized and unanesthetized TG mice and often following an ostensible hyperpolarization of the membrane, which was presumably due to inhibitory input from other activated GABA neurons or terminals in the region.

In both *in vitro* and *in vivo*, pNon-GABA neurons in the LDT/SubLDT region were found to be inhibited with the photostimulation of the pGABA neurons. Given the relatively large size of their soma and spike width, some of these cells were undoubtedly ACh neurons. The remainder are likely glutamate neurons, which overlap in size and spike width with the GABA neurons in the region (Boucetta et al., 2014). Whereas the majority of the pNon-GABA neurons were inhibited by the evoked discharge of the pGABA neurons, a minority were facilitated or presumably disinhibited after some delay. But all neurons recorded *in vivo* in the LDT/SubLDT region altered their firing during the evoked discharge of the pGABA neurons. The effects of the photostimulation in this region cannot therefore be attributed solely to increased discharge of the GABA neurons, but also to altered discharge of all codistributed neurons in the region. Such local network activity changes were also revealed in optogenetic study of the ACh neurons in the LDT/SubLDT (Cisse et al., 2018) and in the basal forebrain where ACh neuronal photostimulation also altered the activity of intermingled GABA neurons (Zant et al., 2016). Since ACh neurons in the LDT/SubLDT give rise to rebound excitation when released from hyperpolarized membrane potentials (Cisse et al., 2018), they would likely burst on release from GABAergic inhibitory input.

←

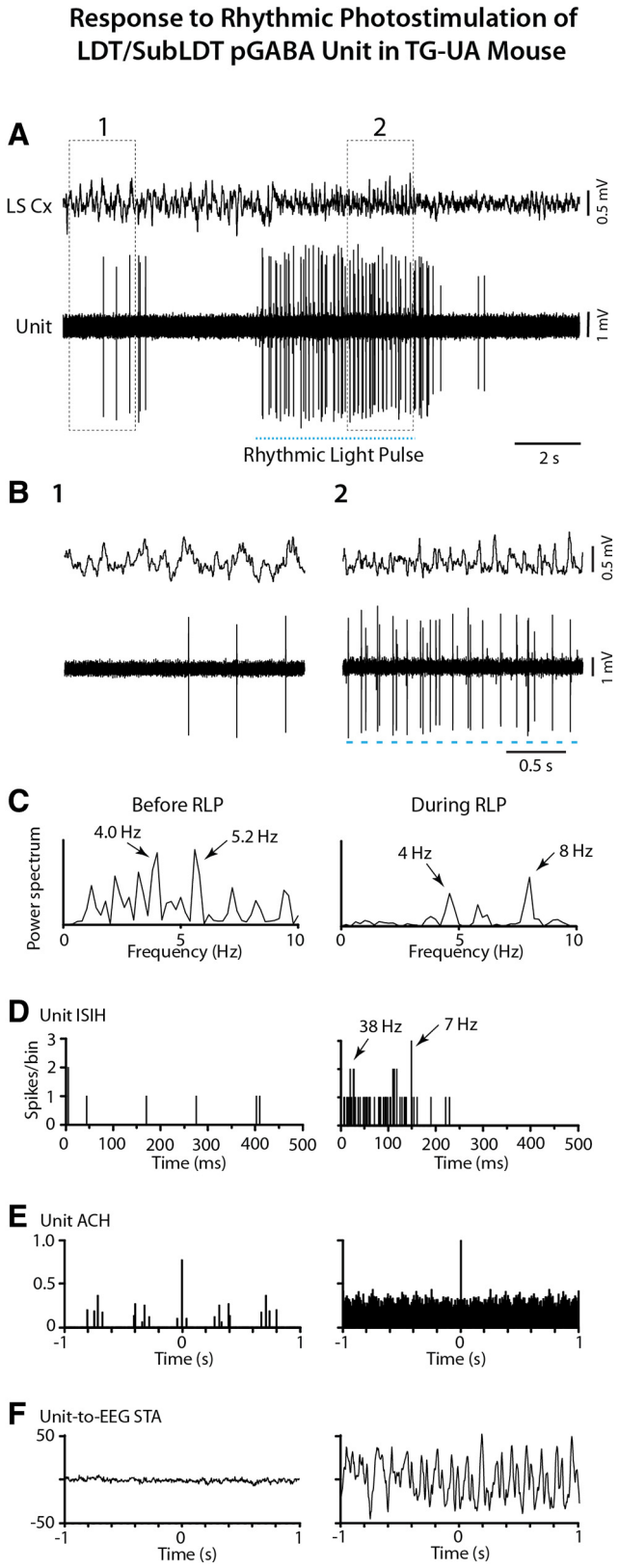

Figure 10. Response of LDT/SubLDT pGABA unit along with EEG to RLP stimulation in a TG-UA mouse (#5 in Mouse CVGAT18 as shown in Fig. 9). ***A***, RLP stimulation at high theta frequency (50 ms, 8 Hz for ~5 s) was delivered during a period of EEG irregular activity. ***B***, As shown in the expanded traces 1 and 2, the pGABA unit was driven by the light pulses to fire phasically during the RLPs, whereas the EEG was progressively driven into a theta-like rhythm. ***C***, Evident in the power spectra, the EEG shifted from irregular activity before the RLPs to high theta activity at 8 Hz during the RLPs. ***D***, In the ISIH, the unit firing appeared variable around a γ frequency (30-80 Hz) in the high-frequency range with recurrence in a low-frequency range around the high theta frequency (6-10 Hz). ***E***, In the ACH, the unit firing showed some rhythmicity at ~8 Hz. ***F***, In the Unit-to-EEG STA, unit activity was cross-correlated with the EEG high theta at ~8 Hz. For graph details and abbreviations, see legend to Figure 6.

Rhythmic bursting by GABA and Non-GABA neurons

Many pGABA neurons were able to follow with high-fidelity brief light pulses up to 50 Hz, as typical of fast-firing neurons. When depolarized by long CLPs, they would attain frequencies in this range with an average ~40 Hz IFF in the anesthetized animals. However, in the unanesthetized mice, the CLPs were less effective in driving fast tonic firing, and tended to elicit bursts or cessation of firing, likely due to inhibitory input from other activated GABA neurons in the region. On the other hand, RLPs at frequencies, typical for low theta (4 Hz) in urethane-anesthetized and high theta (8 Hz) in unanesthetized mice, drove rhythmic phasic firing and bursting in GABA neurons, presumably due to their intrinsic ability to respond to depolarizing pulses with initial rapid firing or bursting from relatively hyperpolarized membrane potentials. Moreover, the pNon-GABA neurons were also driven to discharge at the theta rhythm by firing in antiphase to the GABA neurons, bursting when each RLP stopped and the GABA neurons became silent, likely due to release from inhibition. Such neurons would include the ACh neurons, which also show theta bursting (Cisse et al., 2018).

Influence of GABA and Non-GABA unit firing on EEG activity

Photo-evoked tonic discharge by the GABA neurons in the LDT/SubLDT region tended to diminish EEG slow wave activity while appearing to provoke behavioral arousal in unanesthetized mice. Yet the effect on EEG activity was not that clear-cut since γ activity was also reduced. These results are not dissimilar to those involving chemogenetic stimulation of GABA neurons in the PPT, since this stimulation did not appear to affect EEG activity (Kroeger et al., 2017). Yet, the activation of the GABA neurons could through projections into the pontomedullary reticular formation (Jones, 1990), provoke behavioral arousal, whereas through tonic inhibition of cholinergic LDT/SubLDT neurons, it could prevent enhancement of γ EEG activity, which is promoted by the cholinergic neurons (Cisse et al., 2018).

On the other hand, rhythmic theta photostimulation of the *VGAT-ChR2-EYFP* neurons in the LDT/SubLDT region evoked rhythmic theta discharge of the pGABA neurons and cross-correlated EEG theta on the retrosplenial cortex in both urethane-anesthetized and unanesthetized mice, suggesting that these GABA neurons can stimulate or drive theta activity. Such rhythmic theta discharge by presumed GABA neurons in urethane-anesthetized rats had previously been reported in Gudden's tegmental nuclei, particularly the ventral tegmental nucleus (Kocsis et al., 2001) and in the nucleus incertus (Nunez et al., 2006; Ma et al., 2013). Theta oscillations have also been recorded in presumed GABA neurons in unanesthetized rats during PS in the ventral tegmental nucleus (Bassant and Poindessous-Jazat, 2001) and the dorsomedial tegmental area (DMTg) (Sakai, 2012) and in identified GABA neurons in the SubLDT (Boucetta et al., 2014). It is thus possible that GABA

←

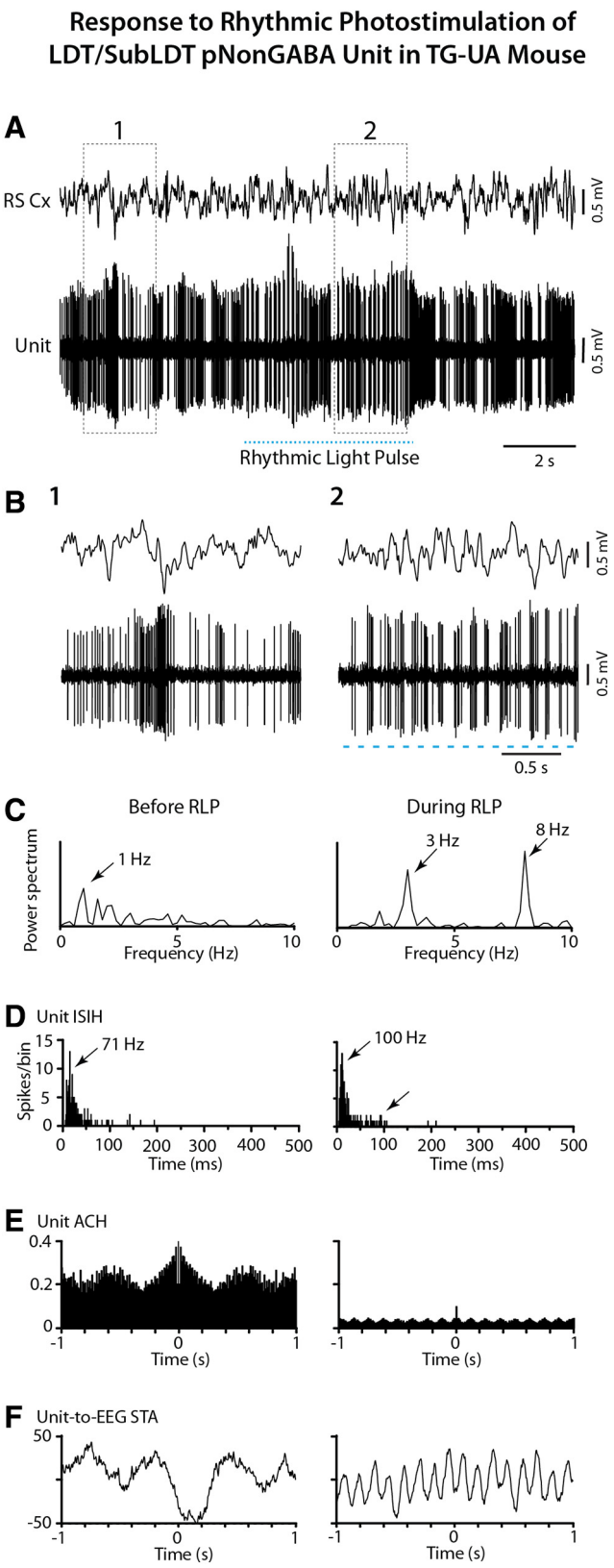

Figure 11. Response of LDT/SubLDT pNon-GABA unit along with EEG to RLP stimulation in a TG-UA mouse (#5 in Mouse CVGAT8). ***A***, RLP stimulation at high theta frequency (50 ms, 8 Hz for ~5 s) was delivered during a period of EEG irregular activity. ***B***, As shown in the expanded traces 1 and 2, the pNon-GABA unit was driven by the light pulses to fire phasically during the off phase of the RLPs, whereas the EEG was progressively driven into a theta-like rhythm. ***C***, Evident in the power spectra, the EEG shifted from irregular activity before the RLPs to high theta activity at 8 Hz during the RLPs. ***D***, In the ISIH, the unit firing was variable and included high-frequency burst-like spiking (~100 Hz) and lower frequency recurrence around a high theta range. ***E***, In the ACH, the unit firing showed weak rhythmicity at ~8 Hz. ***F***, In the Unit-to-EEG STA, unit activity was cross-correlated with the EEG high theta at ~8 Hz. For graph details and abbreviations, see legend to Figure 6.

neurons, distributed through the periventricular region and below within Gudden's tegmental nuclei, nucleus incertus, DMTg, and LDT/SubLDT, have the capacity to discharge rhythmically at a theta frequency and influence theta-related activity in the brain. This influence could occur through ascending projections from GABAergic as well as cholinergic and other PMT neurons (Ford et al., 1995), which project into the hypothalamus and may reach into the mammillary bodies, supramammillary nucleus, anterior thalamic nuclei, basal forebrain, and septum (Satoh and Fibiger, 1986; Ford et al., 1995; Vertes and Kocsis, 1997; Bassant and Poindessous-Jazat, 2001; Ma et al., 2013). Cholinergic and noncholinergic, which would include GABA, neurons also project into the pontomedullary reticular formation (Jones, 1990; Semba et al., 1990), through which they could influence bulbar and spinally projecting neurons and processes involved in rhythmic theta-related sensory-motor processes, including importantly whisking (Grion et al., 2016; Kleinfeld et al., 2016).

Discharge of GABA neurons during natural sleep-wake states

It was found here that GABA neurons in the LDT/SubLDT region discharge maximally during aW and PS while firing at a low rate or not at all during SWS. Moreover, they fire in recurrent bursts in a theta range of frequencies when theta activity appears on the EEG during these states. On the other hand, their firing was not commonly cross-correlated or coupled with the forebrain theta activity recorded from the retrosplenial cortex during aW or PS. Such bursting was also observed in the ACh neurons of the LDT/SubLDT and PPT that was cross-correlated with EEG theta when driven by photostimulation but was not commonly so during natural aW or PS in the head-fixed mice (Cisse et al., 2018). As concluded for the cholinergic neurons, the brainstem phasic activity may not be tightly coupled to theta of the limbic forebrain and could be more closely related to rapid whisker movements and twitching, which are episodic but maximal in association with forebrain theta activity during PS (Mohns and Blumberg, 2008; Tiriac et al., 2012; Del Rio-Bermudez et al., 2017). During waking, rhythmic whisking has been shown to be transiently coupled to limbic theta during exploration (Grion et al., 2016; Kleinfeld et al., 2016). Moreover, phasic discharge cross-correlated with EEG theta rhythm has been described during PS in some identified GABA neurons in the SubLDT (Boucetta et al., 2014) and unidentified, presumed GABA neurons in the DMTg (Sakai, 2012), suggesting that, in some periods or activities, such coherence between brainstem and forebrain theta-related activity may occur in GABA neurons in the LDT/SubLDT region. Collectively, this theta-related bursting in GABAergic and Non-GABAergic, including cholinergic, neurons can contribute to the coordination of sensory-motor systems and consolidation of memory during aW and PS (Mohns and Blumberg, 2008; Tiriac et al., 2012; Boyce et al., 2016; Grion et al., 2016; Kleinfeld et al., 2016; Del Rio-Bermudez et al., 2017; Cisse et al., 2018).

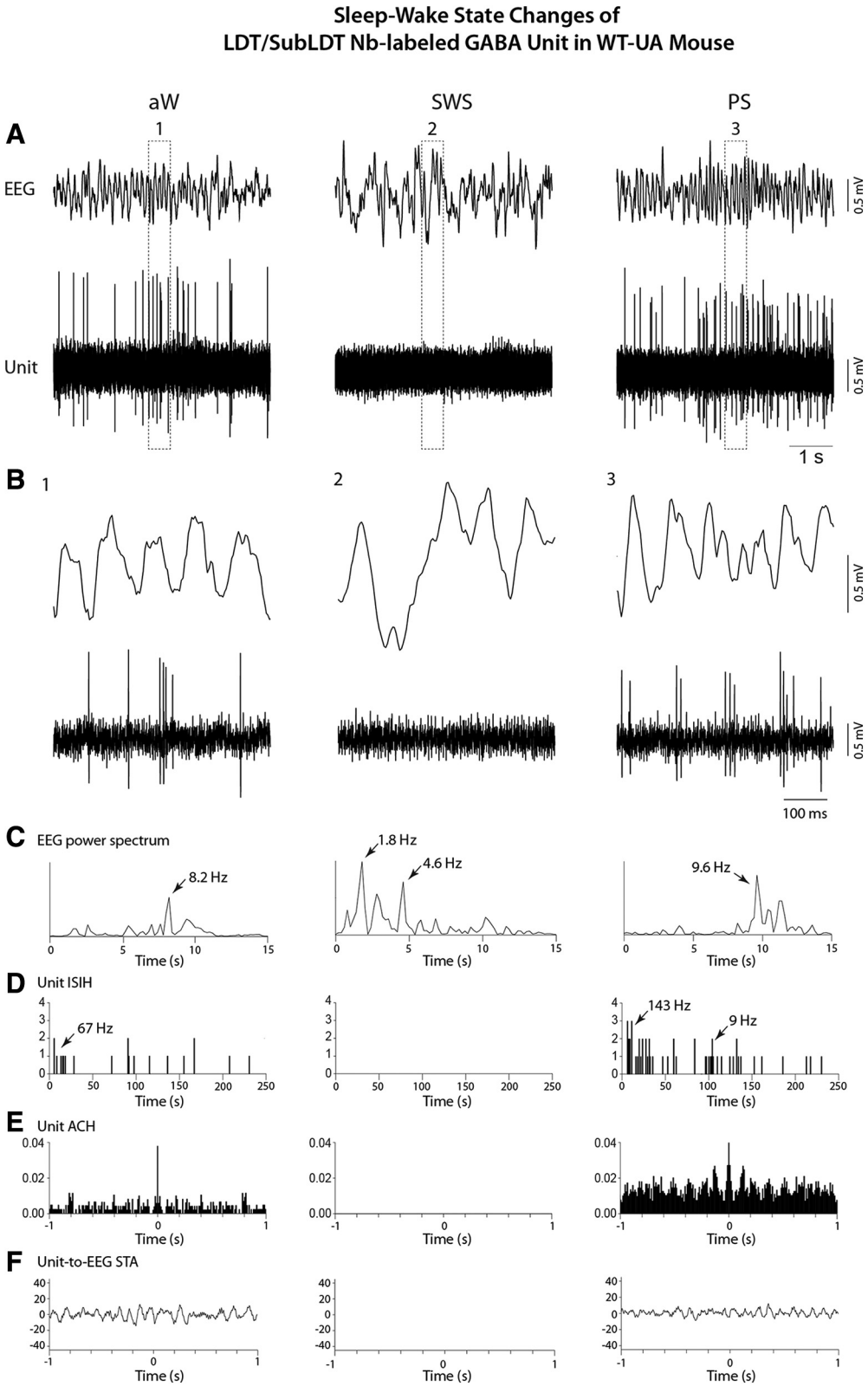

Figure 12. Response of Nb-labeled GABA unit in WT-UA mouse to sleep-wake state changes. ***A***, The unit (#8 in Mouse CWT4) was recorded in association with EEG during aW, SWS, and PS. ***B***, As evident in expanded segments 1, 2, and 3, the unit discharged during aW and PS and was virtually silent during SWS. The pattern of firing reflected phasic burst discharge in association with high theta EEG activity during aW and PS. ***C***, In EEG power spectra, the activity reflected theta activity (at 8.2 Hz) during W, slow wave activity with a peak at 1.8 Hz during SWS, and rhythmic theta at frequencies of >9 Hz (peak at 9.6 Hz) during PS. ***D***, In the Unit ISIH, evidence of bursting activity (mode at 143 Hz) is present with some recurrent spiking (low-frequency mode ~9 Hz) during PS. ***E***, In the Unit ACH, there was minimal indication of rhythmic firing. ***F***, In the Unit-to-EEG STA, there was minimal cross-correlated rhythmic activity with high theta EEG activity of PS. Data analysis was performed on 5 s periods of W, SWS, and PS as illustrated. For graph details and abbreviations, see legend to Figure 6.

References

Bassant MH, Poindessous-Jazat F (2001) Ventral tegmental nucleus of Gudden: a pontine hippocampal theta generator? Hippocampus 11:809–813.

Boucetta S, Jones BE (2009) Activity profiles of cholinergic and intermingled GABAergic and putative glutamatergic neurons in the pontomesencephalic tegmentum of urethane-anesthetized rats. J Neurosci 29:4664–4674.

Boucetta S, Cisse Y, Mainville L, Morales M, Jones BE (2014) Discharge profiles across the sleep-waking cycle of identified cholinergic, GABAergic, and glutamatergic neurons in the pontomesencephalic tegmentum of the rat. J Neurosci 34:4708–4727.

Boyce R, Glasgow SD, Williams S, Adamantidis A (2016) Causal evidence for the role of REM sleep theta rhythm in contextual memory consolidation. Science 352:812–816.

Brown RE, Basheer R, McKenna JT, Strecker RE, McCarley RW (2012) Control of sleep and wakefulness. Physiol Rev 92:1087–1187.

Brown RE, McKenna JT, Winston S, Basheer R, Yanagawa Y, Thakkar MM, McCarley RW (2008) Characterization of GABAergic neurons in rapid-eye-movement sleep controlling regions of the brainstem reticular formation in GAD67-green fluorescent protein knock-in mice. Eur J Neurosci 27:352–363.

Cape EG, Jones BE (2000) Effects of glutamate agonist versus procaine microinjections into the basal forebrain cholinergic cell area upon gamma and theta EEG activity and sleep-wake state. Eur J Neurosci 12:2166–2184.

Cape EG, Manns ID, Alonso A, Beaudet A, Jones BE (2000) Neurotensin-induced bursting of cholinergic basal forebrain neurons promotes gamma and theta cortical activity together with waking and paradoxical sleep. J Neurosci 20:8452–8461.

Cisse Y, Toossi H, Ishibashi M, Mainville L, Leonard CS, Adamantidis A, Jones BE (2018) Discharge and role of acetylcholine pontomesencephalic neurons in cortical activity and sleep-wake states examined by optogenetics and juxtacellular recording in mice. eNeuro 5:ENEURO.0270-18.2018.

Del Cid-Pellitero E, Plavski A, Mainville L, Jones BE (2017) Homeostatic changes in GABA and glutamate receptors on excitatory cortical neurons during sleep deprivation and recovery. Front Syst Neurosci 11:17.

Del Rio-Bermudez C, Kim J, Sokoloff G, Blumberg MS (2017) Theta oscillations during active sleep synchronize the developing rubro-hippocampal sensorimotor network. Curr Biol 27:1413–1424.e4.

El Mansari M, Sakai M, Jouvet M (1989) Unitary characteristics of presumptive cholinergic tegmental neurons during the sleep-waking cycle in freely moving cats. Exp Brain Res 76:519–529.

Erisir A, Lau D, Rudy B, Leonard CS (1999) Function of specific K(+) channels in sustained high-frequency firing of fast-spiking neocortical interneurons. J Neurophysiol 82:2476–2489.

Ford B, Holmes C, Mainville L, Jones BE (1995) GABAergic neurons in the rat pontomesencephalic tegmentum: codistribution with cholinergic and other tegmental neurons projecting to the posterior lateral hypothalamus. J Comp Neurol 363:177–196.

Ganini D, Leinisch F, Kumar A, Jiang J, Tokar EJ, Malone CC, Petrovich RM, Mason RP (2017) Fluorescent proteins such as eGFP lead to catalytic oxidative stress in cells. Redox Biol 12:462–468.

Grion N, Akrami A, Zuo Y, Stella F, Diamond ME (2016) Coherence between rat sensorimotor system and hippocampus is enhanced during tactile discrimination. PLoS Biol 14:e1002384.

Hassani OK, Lee MG, Henny P, Jones BE (2009) Discharge profiles of identified GABAergic in comparison to cholinergic and putative glutamatergic basal forebrain neurons across the sleep-wake cycle. J Neurosci 29:11828–11840.

Inoue T (2018) TI Workbench, an integrated software package for electrophysiology and imaging. Microscopy (Oxf) 67:129–143.

Ishibashi M, Gumenchuk I, Kang B, Steger C, Lynn E, Molina NE, Eisenberg LM, Leonard CS (2015) Orexin receptor activation generates gamma band input to cholinergic and serotonergic arousal system neurons and drives an intrinsic Ca(2+)-dependent resonance in LDT and PPT cholinergic neurons. Front Neurol 6:120.

Jones BE (1990) Immunohistochemical study of choline acetyl transferase-immunoreactive processes and cells innervating the pontomedullary reticular formation. J Comp Neurol 295:485–514.

Jones BE (1991) Paradoxical sleep and its chemical/structural substrates in the brain. Neuroscience 40:637–656.

Jones BE (1993) The organization of central cholinergic systems and their functional importance in sleep-waking states. Prog Brain Res 98:61–71.

Kalmbach A, Hedrick T, Waters J (2012) Selective optogenetic stimulation of cholinergic axons in neocortex. J Neurophysiol 107:2008–2019.

Kamondi A, Williams JA, Hutcheon B, Reiner PB (1992) Membrane properties of mesopontine cholinergic neurons studied with the whole-cell patch-clamp technique: implications for behavioral state control. J Neurophysiol 68:1359–1372.

Kim T, Thankachan S, McKenna JT, McNally JM, Yang C, Choi JH, Chen L, Kocsis B, Deisseroth K, Strecker RE, Basheer R, Brown RE, McCarley RW (2015) Cortically projecting basal forebrain parvalbumin neurons regulate cortical gamma band oscillations. Proc Natl Acad Sci USA 112:3535–3540.

Kleinfeld D, Deschenes M, Ulanovsky N (2016) Whisking, sniffing, and the hippocampal theta-rhythm: a tale of two oscillators. PLoS Biol 14: e1002385.

Kocsis B, Di Prisco GV, Vertes RP (2001) Theta synchronization in the limbic system: the role of Gudden's tegmental nuclei. Eur J Neurosci 13:381–388.

Koike BD, Farias KS, Billwiller F, Almeida-Filho D, Libourel PA, Tiran-Cappello A, Parmentier R, Blanco W, Ribeiro S, Luppi PH, Queiroz CM (2017) Electrophysiological evidence that the retrosplenial cortex displays a strong and specific activation phased with hippocampal theta during paradoxical (REM) sleep. J Neurosci 37:8003–8013.

Kroeger D, Ferrari LL, Petit G, Mahoney CE, Fuller PM, Arrigoni E, Scammell TE (2017) Cholinergic, glutamatergic, and GABAergic neurons of the pedunculopontine tegmental nucleus have distinct effects on sleep/wake behavior in mice. J Neurosci 37:1352–1366.

Lee MG, Hassani OK, Alonso A, Jones BE (2005) Cholinergic basal forebrain neurons burst with theta during waking and paradoxical sleep. J Neurosci 25:4365–4369.

Leonard CS, Llinas RR (1990) Electrophysiology of mammalian pedunculopontine and laterodorsal tegmental neurons *in vitro*: implications for the control of REM sleep. In: Brain cholinergic systems (Steriade M, Biesold D, eds), pp 205–223. Oxford: Oxford UP.

Ma S, Blasiak A, Olucha-Bordonau FE, Verberne AJ, Gundlach AL (2013) Heterogeneous responses of nucleus incertus neurons to corticotrophin-releasing factor and coherent activity with hippocampal theta rhythm in the rat. J Physiol 591:3981–4001.

Maloney KJ, Cape EG, Gotman J, Jones BE (1997) High-frequency gamma electroencephalogram activity in association with sleep-wake states and spontaneous behaviors in the rat. Neuroscience 76:541–555.

Manns ID, Alonso A, Jones BE (2000) Discharge properties of juxtacellularly labeled and immunohistochemically identified cholinergic basal forebrain neurons recorded in association with the electroencephalogram in anesthetized rats. J Neurosci 20:1505–1518.

Mohns EJ, Blumberg MS (2008) Synchronous bursts of neuronal activity in the developing hippocampus: modulation by active sleep and association with emerging gamma and theta rhythms. J Neurosci 28:10134–10144.

Nagel G, Szellas T, Huhn W, Kateriya S, Adeishvili N, Berthold P, Ollig D, Hegemann P, Bamberg E (2003) Channelrhodopsin-2, a directly light-gated cation-selective membrane channel. Proc Natl Acad Sci USA 100:13940–13945.

Nunez A, Cervera-Ferri A, Olucha-Bordonau F, Ruiz-Torner A, Teruel V (2006) Nucleus incertus contribution to hippocampal theta rhythm generation. Eur J Neurosci 23:2731–2738.

Paxinos G, Franklin KB (2001) The mouse brain in stereotaxic coordinates, Ed 2. San Diego: Academic.

Pinault D (1996) A novel single-cell staining procedure performed *in vivo* under electrophysiological control: morpho-functional features of juxtacellularly labeled thalamic cells and other central neurons with biocytin or Neurobiotin. J Neurosci Methods 65:113–136.

Sakai K (2012) Discharge properties of presumed cholinergic and noncholinergic laterodorsal tegmental neurons related to cortical activation in non-anesthetized mice. Neuroscience 224:172–190.

Satoh K, Fibiger HC (1986) Cholinergic neurons of the laterodorsal tegmental nucleus: efferent and afferent connections. J Comp Neurol 253:277–302.

Semba K, Reiner PB, Fibiger HC (1990) Single cholinergic mesopontine tegmental neurons project to both the pontine reticular formation and the thalamus in the rat. Neuroscience 38:643–654.

Steriade M, Datta S, Pare D, Oakson G, Dossi RC (1990) Neuronal activities in brain-stem cholinergic nuclei related to tonic activation processes in thalamocortical systems. J Neurosci 10:2541–2559.

Steriade M, Dossi RC, Nuñez A (1991) Network modulation of a slow intrinsic oscillation of cat thalamocortical neurons implicated in sleep delta waves, cortically induced synchronization and brainstem cholinergic suppression. J Neurosci 11:3200–3217.

Ting JT, Daigle TL, Chen Q, Feng G (2014) Acute brain slice methods for adult and aging animals: application of targeted patch clamp analysis and optogenetics. Methods Mol Biol 1183:221–242.

Tiriac A, Uitermarkt BD, Fanning AS, Sokoloff G, Blumberg MS (2012) Rapid whisker movements in sleeping newborn rats. Curr Biol 22:2075–2080.

Vertes RP, Kocsis B (1997) Brainstem-diencephalo-septohippocampal systems controlling the theta rhythm of the hippocampus. Neuroscience 81:893–926.

Wang HL, Morales M (2009) Pedunculopontine and laterodorsal tegmental nuclei contain distinct populations of cholinergic, glutamatergic and GABAergic neurons in the rat. Eur J Neurosci 29:340–358.

Zant JC, Kim T, Prokai L, Szarka S, McNally J, McKenna JT, Shukla C, Yang C, Kalinchuk AV, McCarley RW, Brown RE, Basheer R (2016) Cholinergic neurons in the basal forebrain promote wakefulness by actions on neighboring non-cholinergic neurons: an opto-dialysis study. J Neurosci 36:2057–2067.

Zhao S, Ting JT, Atallah HE, Qiu L, Tan J, Gloss B, Augustine GJ, Deisseroth K, Luo M, Graybiel AM, Feng G (2011) Cell type-specific channelrhodopsin-2 transgenic mice for optogenetic dissection of neural circuitry function. Nat Methods 8:745–752.